Quaternary Science Reviews 201 (2018) 124–146

Contents lists available at ScienceDirect

Quaternary Science Reviews

journal homepage: www.elsevier.com/locate/quascirev

Postglacial relative sea-level histories along the eastern Canadian coastline

Matteo Vacchi [a, *], Simon E. Engelhart [b], Daria Nikitina [c], Erica L. Ashe [d, e, f], W. Richard Peltier [g], Keven Roy [h, i], Robert E. Kopp [d, f], Benjamin P. Horton [h, i, j]

[a] Geography, College of Life and Environmental Sciences, University of Exeter, EX4 4RJ, UK
[b] Department of Geosciences, University of Rhode Island, Kingston, RI, 02881, USA
[c] Department of Earth and Space Science, West Chester University of Pennsylvania, West Chester, PA, 19383, USA
[d] Institute of Earth, Ocean, and Atmospheric Sciences, Rutgers University, New Brunswick, NJ, 08901, USA
[e] Department of Statistics and Biostatistics, Rutgers University, Piscataway, NJ, 08854, USA
[f] Department of Earth and Planetary Sciences, Rutgers University, Piscataway, NJ, 08854, USA
[g] Department of Physics, University of Toronto, Toronto, Canada
[h] Asian School of the Environment, Nanyang Technological University, 639798, Singapore
[i] Earth Observatory of Singapore, Nanyang Technological University, 639798, Singapore
[j] Department of Marine and Coastal Sciences, Rutgers University, New Brunswick, NJ, 08901, USA

ARTICLE INFO

Article history:
Received 12 January 2018
Received in revised form
7 September 2018
Accepted 28 September 2018

Keywords:
Sea-level change
Glacial isostatic adjustment
Atlantic Canada
Hudson Bay
Holocene

ABSTRACT

We have assembled a database of Relative Sea Level (RSL) data points from the eastern coast of Canada from Hudson Bay to the border with the USA. In compiling this database we have critically reviewed 1092 radiocarbon dated samples from raised beaches, isolation basins, intertidal and marine deposits, and archaeological indicators to produce 405 sea-level index points and 687 sea-level limiting points. Our comprehensive, systematic, and quality-controlled RSL database allowed for the reconstruction of the postglacial evolution of 34 regions of eastern Canada providing new basin-scale insights into the processes driving RSL changes in the last ~16 ka. The combination of a database of sea-level index points with an innovative empirical-Bayesian spatio-temporal statistical model provided new insights into rates and magnitude of the spatially-variable glacial isostatic adjustment (GIA), which dominated the postglacial RSL evolution in this sector of North America. A continuous postglacial RSL fall is observed at latitudes $\geq$ ~50° N with higher rates (up to 35 mm a^{-1}) recorded in southeastern Hudson Bay. At lower latitudes, the evolution is non-monotonic with RSL that dropped to a spatially variable early-Holocene lowstand, followed by a mid-Holocene highstand and, eventually, a gradual drop to present RSL. This pattern is particularly evident in the St Lawrence corridor. Along the majority of the Newfoundland, New Brunswick and western Nova Scotia coasts, a late-Pleistocene/early-Holocene RSL lowstand was followed by a continuous rise through the Holocene. At the margin of the former ice-sheet (i.e. eastern Nova Scotia), our data identify a continuous RSL rise through the Holocene. These records are characterized by decreasing rates of RSL rise through time, commencing with a rapid rise during the early Holocene (up to ~17 mm a^{-1}), a slowdown in the mid-Holocene (average rates $\leq$ ~9 mm a^{-1}), and a further reduction in the late Holocene (average rates < 2 mm a^{-1}). Finally, our database allowed the identification of regions, including the Labrador coast and part of the St Lawrence corridor, where further investigations are required to better constrain the RSL evolution and improve our ability to assess the variability of RSL histories.

© 2018 Published by Elsevier Ltd.

1. Introduction

The last transition between glacial and interglacial climatic conditions (between ~26 and 10 ka BP; Peltier and Fairbanks, 2006) produced a dramatic global sea-level response. Regions distant from the major glaciation centres (termed far-field) were characterized by a relative sea-level (RSL) rise of ~120–130 m since the Last Glacial Maximum (LGM) due, largely, to the influx of ~50 million km^3 of land-based ice into the oceans (e.g., Fleming et al.,

* Corresponding author.
E-mail address: m.vacchi@exeter.ac.uk (M. Vacchi).

https://doi.org/10.1016/j.quascirev.2018.09.043
0277-3791/© 2018 Published by Elsevier Ltd.

1998; Peltier and Fairbanks, 2006; Khan et al., 2015). However, RSL dropped by many hundreds of metres in regions once covered by the major ice-sheets (termed near-field) as a consequence of the isostatic 'rebound' of the solid Earth (Peltier, 1998; Milne et al., 2001; Whitehouse et al., 2012). Geophysical models can simulate the GIA process (e.g., Clark et al., 1978; Milne et al., 1999; Tarasov and Peltier, 2004; Simon et al., 2016). However, data is needed to both constrain the models and to test the accuracy of predictions made using them (e.g., Han and Gomez, 2018). Although instrumental (e.g., GPS, tide gauges, satellite altimetry) data are used to constrain GIA models (e.g., Milne et al., 2004; Stocchi and Spada, 2009; Peltier et al., 2015), the most commonly used data are geological records of postglacial RSL obtained from coastal deposits (such as beach ridges or salt-marshes; e.g., Gehrels et al., 2004; Simon et al., 2014; Sander et al., 2016), because they provide estimates of RSL changes prior to the post-industrial acceleration (e.g., Engelhart et al., 2009) and minimize the influence of anthropogenic processes (e.g., Karegar et al., 2016). By comparing RSL data to GIA predictions, it is possible to infer parameters relating to changes in climate (e.g., Peltier, 1998; Tarasov and Peltier, 2004; Dutton et al., 2015), regional ice-sheet variations (e.g., Peltier, 2002; Shennan et al., 2006), the rate and geographic source of meltwater influx (e.g. Peltier, 2002; Mitrovica and Milne, 2002; Bradley et al., 2016), and the rheological structure of the solid Earth (e.g. Wu and Peltier, 1982, 1984; Peltier, 1998; Lambeck et al., 2014; Roy and Peltier, 2015), a key parameter for understanding mantle flow and the tectonic evolution of our planet. However, data must be standardized according to a common framework to ensure that the models are tested against accurate and comparable datasets (e.g., Shennan and Horton, 2002; Shennan et al., 2015).

Postglacial regional RSL databases consisting of sea-level index points (SLIP) and sea-level limiting points have been compiled from the United States (e.g., Engelhart and Horton, 2012; Engelhart et al., 2015), Caribbean and South America (e.g., Milne and Peros, 2013; Khan et al., 2017), Mediterranean (e.g., Vacchi et al., 2014, 2016), southeast Asia (e.g., Woodroffe and Horton, 2005), China (e.g., Zong, 2004), and northern European coasts (e.g., Shennan and Horton, 2002; Brooks and Edwards, 2006; Vink et al., 2007). Significant compilation efforts have been undertaken in eastern Canada to reconstruct the variability of maximal and minimal sea-level stands along the Canadian coastlines (e.g., Andrews, 1973; Shaw and Forbes, 1995; Dyke and Peltier, 2000; Dyke, 2004; Dyke et al., 2005). However, the data need to be systematically assessed using the standardized approach to produce SLIPs and limiting data (e.g., Shennan et al., 2015; Hijma et al., 2015) using the latest radiocarbon calibration curves (e.g., Reimer et al., 2013).

At the LGM, eastern Canada was entirely covered by the Laurentide Ice-sheet (LIS), the thickness of which according to the ICE-6G_C (VM5a) model of Peltier et al. (2015) is depicted in Fig. 1A. The presence of a multitude of raised shorelines and marine deposits led to the recognition of a location dependent maximum postglacial marine limit altitude (Dyke et al., 2005) and to documentation of the progressive formation of both the Tyrrel and Champlain seas (e.g., Matthews, 1966; Andrews and Falconer, 1969; Prest, 1970; Hillaire-Marcel and Occhietti, 1977; Hillaire-Marcel and Fairbridge, 1978; Gray et al., 1980; Dyke and Prest, 1987; Dionne, 1988; Barber et al., 1999; Dyke et al., 2005; Bell et al., 2005). In particular, radiocarbon and surface exposure dating have been used to date the retreat of the LIS, to reconstruct the RSL response to glacial unloading, and to assess coastline modifications since the LGM (e.g., Hillaire-Marcel, 1976; Dyke and Prest, 1987; Clark and Fitzhugh, 1990; Parent and Occhietti, 1988; Stea and Mott, 1989, Gray et al., 1993; Dyke, 2004; Lajeunesse and Allard, 2003). Building off its dataset, Dyke (2004) compiled a large database of radiocarbon dates in North America to provide constraints on ice retreat in the region with more recent surface exposure dates providing further information (e.g., Carlson et al., 2007; Stokes et al., 2009).

To serve the purpose of providing an improved database for GIA model development, we have compiled data from raised beaches, isolation basins, intertidal and marine deposits and archaeological indicators to produce 1092 SLIPs and limiting points for 34 regions located along the eastern Canadian coast. To produce the SLIPs along with their associated uncertainty, we followed the protocol described by International Geoscience Programme (IGCP) projects 61, 200, 495, 588, and 639 (e.g., Preuss, 1979; van de Plassche, 1982; Gehrels and Long, 2007; Horton et al., 2009; Shennan et al., 2015; Padgett et al.., 2018). Our comprehensive and quality controlled RSL database for eastern Canada combines data from different geomorphological contexts to obtain insights into the processes driving postglacial RSL changes. The data improves constaints on the spatial variability of GIA and its role in the RSL evolution of the area. The application of an innovative empirical-Bayesian spatio-temporal statistical model provided new insights into rates and magnitude of the postglacial RSL changes in this key region.

2. The eastern Canadian coastline

The study area encompasses the Atlantic and Hudson Bay coasts of Canada at latitudes between 62.6°N and 43.7°N and longitudes between −52.0°E and −94.0°E (Fig. 1A and B). The eastern Canadian database excludes the Arctic, but includes SLIPs collected along more than 10,000 km of Canadian coastline from 16 to 0 ka BP. To account for spatial variability of RSL changes, we clustered the data into 34 regions, which experienced different ice loading and deglaciation histories (Dyke, 2004; Dyke et al., 2005). Further, in areas characterized by comparable deglaciation chronology, we accounted for the geographical proximity of the data, the distance from the former ice domes, and the reconstructed thicknesses of the LIS (Fig. 1A). The database is structured such that future users can make their own judgements on using our regions, delineating their own, or choosing not to use set regions at all (e.g., Vacchi et al., 2016).

2.1. Hudson Bay (regions #1 to #7)

Hudson Bay is a relatively shallow (mean depth of ~150 m) semi-enclosed sea connected with the Atlantic Ocean through the Hudson Strait (Arbic et al., 2007; Griffiths and Peltier, 2009; Webb, 2014, Fig. 1B). It has a spatially variable tidal regime (e.g., Webb, 2014) with Great Diurnal Range (GT) decreasing from ~4 m along the western coast to ~1.5 m along the eastern coast.

We subdivided Hudson Bay into seven regions according to the deglaciation pattern and the geographical position of the RSL datapoints. NW Hudson Bay (1), located in southeastern Nunavut, deglaciated between ~8.0 and ~7.7 ka, associated with the maximal extent of the Tyrrel Sea transgression with a paleo-shoreline at this time that was ~150 km inland compared to present (Peltier, 1998; Dyke, 2004; Simon et al., 2014). Mid-western Hudson Bay (2) is located in northwestern Manitoba.

We subdivided James Bay (southern Hudson Bay, northern Ontario, western Quebec) into western (3) and eastern (4) James Bay. The ice cover lasted ~0.5 ka longer in western than in eastern James Bay, which was already flooded by the Tyrrel Sea at ~8.45 ka (Dyke, 2004). Southeast Hudson Bay region (5) encompasses a large portion of western Quebec ranging from Boniface River to Poste de la Baleine. This region is located within ~250 km of the Quebec-Labrador ice dome, and deglaciated after ~8.4 ka. Although a comparable deglacial history occurred in the mid-eastern Hudson Bay (6) and northeastern Hudson Bay (7) regions, there is a difference in ice thicknesses at the LGM (Peltier et al., 2015). The Tyrrel

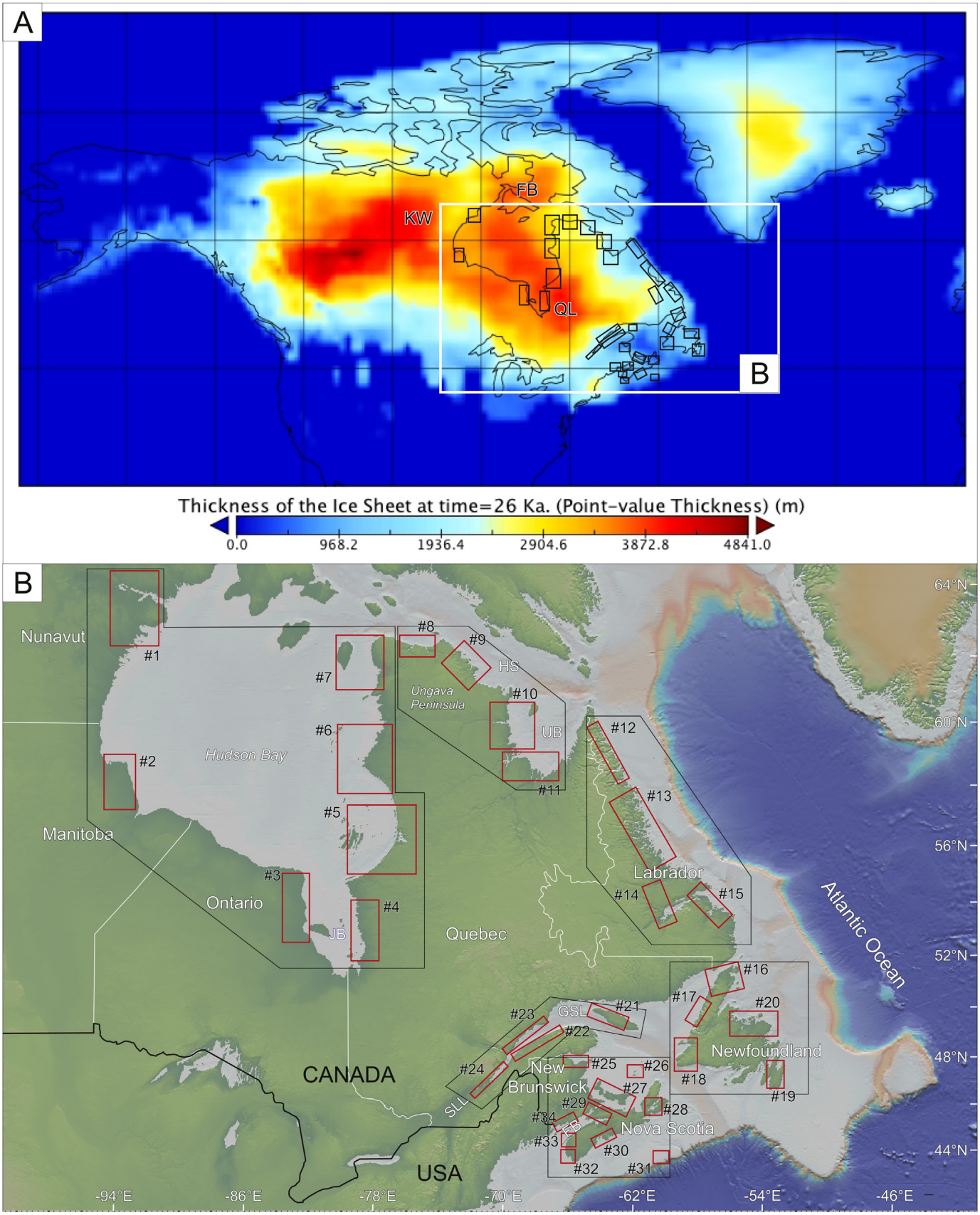

Fig. 1. (A) Approximate spatial extent and ice thickness of the Cordilleran and Laurentide ice-sheets at the LGM redrawn after Roy and Peltier (2017). KW is the Keewatin ice dome, QL is the Quebec-Labrador ice dome and FB is the Foxe basin ice dome. (B) Location of sea-level data of this paper grouped into sector (black polygons) and regions (red rectangles) as explained in text. JB is the James Bay, HS is the Hudson Strait, UB is Ungava Bay, GSL is the Gulf of St. Lawrence, SLL are the St. Lawrence lowlands and FB is the Bay of Fundy. (For interpretation of the references to colour in this figure legend, the reader is referred to the Web version of this article.)

Sea remained at the northernmost limit of both these regions from ~9.0 to ~8.4 before it flooded the whole sector at ~8.0 ka. Given the slight variations in the radiocarbon dates along the coast of Hudson Bay and the dependence of these dates upon the marine reservoir correction, one might reasonably assume that the Bay became connected to the Atlantic Ocean at approximately the same time (Dyke and Prest, 1987; Barber et al., 1999; Clarke et al., 2004), although ice would still have remained grounded at that time in many coastal locations.

2.2. Ungava Peninsula (regions #8 to #11)

Ungava is the northernmost peninsular sector of Quebec (Fig. 1B). The peninsula is a rocky plateau characterized by several lakes and bounded by the Hudson Strait to the north and by the Hudson and the Ungava bays to the west and east, respectively (Fig. 1B, Daigneault, 2008). Tidal ranges increase eastwards (Arbic et al., 2007; Webb, 2014) with GT values ranging from ~4 m in the western Hudson strait to more than 12 m in Ungava Bay.

Transgression of the Tyrrel Sea at the Ungava Peninsula was not uniform (Dyke, 2004) with sites located in its northernmost portion (Hudson strait) flooded ~1.0 ka before those in the southeast (Ungava Bay). Further, there is a significant reduction in the ice thickness at the LGM from NW-SE (Fig. 1A). Therefore, we subdivided this sector into four regions (Fig. 1B). The western Hudson strait region (8) is located along the southern coast of Hudson strait. This region was fully deglaciated by ~9.0 ka and was soon after flooded by the Tyrrel Sea, ~0.4 ka before the flooding that occurred in the eastern Hudson strait region (9) and ~1.0 ka before that in the NW Ungava Bay region (10). A further difference in deglacial history is documented at South Ungava Bay (11). Here the ice cover lasted longer, with the whole area reported as flooded by the Tyrrel Sea from ~7.5 ka (Dyke, 2004).

2.3. Labrador (regions #12 to #15)

The Labrador coast encompasses the easternmost portion of the Canadian Shield (Fig. 1B). Cliffs and deep fjords characterize much of the Labrador coastlines where a broad continental shelf extends up to 200 km offshore (e.g. Fillon, 1975). Tidal ranges show little variability along the coastline with GT values that do not exceed 2.5 m.

In contrast to the Ungava peninsula regions, the Labrador coastline is characterized by less variability in deglacial history. However, due to its large geographical extent (~900 km), we subdivided it into four regions. The Northern Labrador region (12) spans from ~60° to ~58.2° N. This sector was entirely ice-covered until ~13 ka and remained close to the periphery of the ice-sheet up to ~10.7 ka. At ~9.5 ka, most of the coast was ice-free (Dyke, 2004). Even if characterized by a comparable deglacial pattern, we preferred to group the RSL data found between ~57.5° and ~54.5° N in the Mid-Labrador region (13).

The ice-sheet covered the entire southern Labrador coast (i.e. at latitudes <54.5° N) until ~11.5 ka. A progressive deglaciation started from the shoreline at ~11.0 ka and reached the most internal sector by ~8.6 ka. Therefore, we subdivide this sector into two regions: the Goose Bay region (14), which was not fully deglaciated until ~8.0 ka and the coastline of the southern Labrador region (15), which was already free of ice at ~10.2 ka.

2.4. Newfoundland (regions #16 to #20)

Newfoundland Island is separated from Labrador by the Strait of Belle Isle in the northwest and is bordered by the Grand Banks in the southeast (Shaw and Potter, 2015, Fig. 1B). In the northeast, cliffs alternate with numerous fjords, river valleys, tidal inlets and barrier beach systems (Forbes, 1984). Tidal range along the Newfoundland coastline is characterized by GT values between ~1 and ~2 m on the northern shores increasing up to ~2.5 m on the southern and western shores. Sea-level indicators are derived predominantly from the numerous small salt-marshes (Shaw and Forbes, 1995; Daly et al., 2007; Kemp et al., 2017). Shaw et al. (2006) underlined the major role played by ice-streams in controlling the ice retreat pattern in this sector of Atlantic Canada. Further, a N-S gradient of the sea level lowstand is reported along the coast of Newfoundland (e.g., Shaw and Potter, 2015).

Following several previous RSL compilations (e.g., Bell et al., 2005; Daly et al., 2007), we subdivided Newfoundland into five regions (Fig. 1B). NW Newfoundland region (16) includes all data above ~50°N with sites being coevally ice free by ~14 ka. The mid-west Newfoundland region (17) encompasses a large sector of the western coast (from ~50° to ~49° N) and became ice-free at ~14.8 ka with an RSL lowstand between 0 and -10 m reported for the area (Shaw and Potter, 2015). The SW Newfoundland region (18) includes the remaining part of the western coast (i.e. at latitudes <49° N) and the western part of the southern coast of the Island. Deglaciation of this entire coastal sector was complete by ~14 ka. The eastern Newfoundland region (19) encompasses the Avalon Peninsula where ice retreat began ~11.4 ka, later than the remaining coastal sector of Newfoundland (Brown MacPherson, 1996). The northeastern Newfoundland region (20) includes data from Notre Dame Bay to western Bonavista Bay. Deglaciation started at ~14.8 ka and the entire region was ice free by ~14.1 ka.

2.5. St. Lawrence corridor (regions #21 to #24)

The St. Lawrence corridor ranges from the St. Lawrence River Lowland to the Gulf of St. Lawrence including Anticosti Island (Fig. 1A and B). The St Lawrence River estuary extends from Quebec City to the eastward end of the Gaspé Peninsula, where it is connected through a slope break with the Laurentian channel, a long sub-horizontal topographic depression interpreted to be the result of a pre-Quaternary drainage system subsequently overdeepened by successive glaciations (Cauchon-Voyer et al., 2008). Tidal range shows variability with GT values that exceed ~5.5 m in the inner part of the estuary (Dionne, 1988) and decrease to ~3 m in the outer part and at Anticosti Island. The Charlevoix Seismic Zone (CSZ), located in the upper St Lawrence estuary, represents the sole noticeable seismically active area of eastern Canada, being historically affected by large earthquakes (i.e. up to M7; Fereidoni and Atkinson, 2015). Sea-level indicators are derived from large salt-marsh zones, muddy tidal flats and gravelly beaches bordered by rocky and sandy cliffs (e.g. Dionne and Coll, 1995; Dionne, 1988, 1990).

The St. Lawrence corridor channelized a major ice stream, which became a major feature of the southeast sector of the Laurentide ice-sheet during its progressive retreat and the consequent transgression of the Champlain Sea (e.g., Dionne, 1977; Occhietti et al., 2001; Dyke, 2004). We subdivide this sector into four regions on the basis of variable deglacial patterns. The Anticosti Island region (21) in the centre of the Gulf of St Lawrence was partly covered by the ice-sheet until ~16.8 ka. Marine transgression started soon after and flooded the whole coastal sector of the island at ~16.2 ka. Even if the distance between the two sides of the lower estuary is < 60 km, a discrepancy between the deglaciation pattern of the northern and the southern coast of St Lawrence estuary is nevertheless documented. The southern St. Lawrence region (22) includes a large portion of the lower estuary (Fig. 1B). Here, the marine transgression is documented between ~14.4 and ~14.1 ka, while in the northern St Lawrence region (23), placed on the

opposite bank of the river, the Champlain Sea had flooded the entire coast by ~12.6 ka. In the inner St. Lawrence region (24), we grouped the data points collected on both sides of the middle to inner portion of the estuary near Quebec City. In this region, the transgression by the Champlain Sea flooded the entire area between ~13.4 and ~13.0 ka.

2.6. New Brunswick and Nova Scotia (regions #25 to #34)

The coastline of New Brunswick and Nova Scotia (Fig. 1B) has a highly variable tidal regime and can be subdivided into three subregions (e.g., Shaw et al., 1993): the microtidal Gulf of St. Lawrence and Northumberland Strait shores (e.g., Scott et al., 1981), with GT values that do not exceed ~1.5 m, the tide-dominated Bay of Fundy shores where GT values may reach ~16 m (e.g., Gehrels et al., 1995; Shaw and Ceman, 1999; Shaw et al., 2010) and the mesotidal eastern Nova Scotia coast where GT values up to ~2.5 m (e.g., Shaw et al., 1993; Gehrels et al., 2004) are recorded. Salt-marshes are common in the low-lying coastal embayments that alternate with rocky headlands (Rampton et al., 1984; Shaw et al., 1993).

At the LGM, this coastal sector represented the southeastern limit of the Laurentide ice-sheet with ice thicknesses mostly lower than 1.5 km. Consequently, most of this area was ice free earlier than the majority of other regions in the database. In the regional subdivision, we have also accounted for the tidal regime, which resulted in the subdivision of the area into nine regions.

In region 25, data points from Chaleur Bay and the Acadian Peninsula were combined. Here deglaciation started at ~14.5 ka, and the entire area was ice-free by ~14.1 ka. The Magdalen Islands region (26) includes data points collected along the coast of a small archipelago placed in the middle of the Gulf of St Lawrence. Here ice lasted until ~14.1 ka, while at ~13.5 ka the whole archipelago was ice-free. The Northumberland Strait region (27) includes data points from both sides of the Northumberland Strait and the northern coast of Prince Edward Island. First evidence of deglaciation is documented at ~14.1 ka in the western portion of the region followed by a significant re-expansion of the ice-caps between ~13.0 and ~12.7 ka (likely triggered by the younger Dryas cooling), most notably in Prince Edward Island. This sector was totally ice free after ~12.0 ka. The Cape Breton Island region (28) includes data points from different sites of Lake Bras D'Or located in the central portion of the Island. Here, first evidence of deglaciation is reported between ~15.2 and ~14.4 ka. In the northeastern Bay of Fundy region (29), we grouped together the data points that were collected primarily in the tidal marshes of Chignecto Bay and Minas Basin. Here, the deglaciation started progressively from ~16.2 ka. The eastern Nova Scotia region (30) was entirely ice free by ~14.1 ka. Located ~200 km offshore of Nova Scotia, the Sable Island region (31) is at the edge of the wide continental shelf of eastern Canada. In this region, located at the extreme edge of the former ice-sheet, deglaciation was early and rapid and became totally ice free at ~20.0 ka. The southern Nova Scotia region (32) deglaciated between ~15.2 and ~14.1 ka. Ice coverage lasted longer (i.e. ~13.45 ka) in the western Nova Scotia region (33) encompassing the lower shore of the Bay of Fundy. The southern New Brunswick region (34) is located along the upper shore of the Bay of Fundy and at the border with the USA. In this region, deglaciation was already complete by ~15.6 ka.

3. Compilation of the relative sea-level database

3.1. Sea-level indicators

We have employed a wide range of sea-level indicators to produce SLIPs and limiting points along the eastern Canadian coastline. Three criteria must be met for a sea-level indicator to be identified as a SLIP or a limiting point: (1) location of the indicator; (2) the calibrated age of the indicator; and (3) the indicative meaning of the indicator (Table 1). The indicative meaning is composed of a reference water level that defines the relation of that indicator to a contemporaneous tide level, such as mean high water (MHW) or mean tide level (MTL); and the indicative range, which is the elevational range occupied by a sea-level indicator (Shennan, 1986). Because sea-level histories are not reconstructed from a single type of indicator, each indicator is related to its own reference water level (Shennan et al., 2015). The reference water level is given as a mathematical expression of tidal parameters rather than as a single elevation $\pm$ a constant, because of the different tidal inundation characteristics among locations of eastern Canada that have micro- to macro-tidal ranges (van de Plassche, 1982).

The majority of SLIPs in our database are derived from salt-marsh sea-level indicators (Table 1). For these indicators, we estimated the indicative meaning using the modern analogues of salt-marsh zonation of vegetation and/or microfossil assemblages (e.g., Scott and Medioli, 1982; Daly et al., 2007; Kemp et al., 2017). The indicative range associated with indicators of salt-marsh origin is from HAT (Highest Astronomic Tide) to MTL (Mean Tidal Level, e.g., Engelhart and Horton, 2012). For indicators from high marsh, higher high marsh or low marsh depositional environments, the associated indicative range is restricted to HAT-MHW (Mean High Water), to HAT-MHHW (Mean Higher High Water) and to MHW-MTL, respectively (Engelhart and Horton, 2012).

In the St. Lawrence Estuary, most of the indicators were from the French literature in which a different nomenclature was employed to describe depositional facies of intertidal sediments (e.g. Dionne, 1997, 1999; Dionne and Coll, 1995). The *shorre* facies has an indicative range from HAT to MTL while the *slikke* facies have an indicative range from MTL to MLLW (Mean Lower Low Water). Indicators listed as lower *shorre* to *slikke*, (e.g., Dionne and Coll, 1995) have an indicative range from MHW to MLLW (Table 1).

Isolation basins provided additional SLIPs (e.g., Pienitz et al., 1991; Miousse et al., 2003; Pendea et al., 2010). Isolation basins are natural rock depressions that were, at different times in their history, isolated from, or connected to, the sea (e.g., Lloyd, 2000; Long et al., 2011). When RSL exceeded the elevation of a basin sill, the basin was inundated by marine water. Conversely, when RSL was lower than the sill, the basin was isolated from the sea and freshwater sediment was deposited. Isolation of a basin caused by falling RSL is recorded in basin sediment by a change from marine to freshwater deposits. The age of basin isolation is estimated by dating the contact between marine and freshwater sediment. We conservatively estimate an indicative range for the transition from marine to freshwater sediment to be HAT to MTL (Engelhart et al., 2015) for both ingress and regress. The height of RSL at the time of isolation is constrained by the sill elevation (Horton et al., 2013a).

Beach deposits (including raised beach ridges) have provided important insights concerning the RSL histories. However, defining an indicative meaning is difficult, notably for beach ridges whose formation zone can range from subtidal to supratidal (e.g., Anthony, 2008; Rovere et al., 2016). Here, SLIPs were primarily produced for beach ridges where they were largely dominated by *Mytilus edulis* shells (e.g. Allard and Tremblay, 1983; Lavoie et al., 2012). This species lives in intertidal to shallow subtidal environments attached to the rock surface or to gravel and is often found deposited in the beach material transported by storm waves (e.g., Petersen, 1986; Gosling, 1992; Lavoie et al., 2012). Modern beach ridge formations in Eastern Canada reported up to 3 m above MTL (Hill et al., 2003; Lavoie et al., 2012; Billy et al., 2015). However, we cannot exclude the possibility that a more intense storm regime may have been able to deposit beach ridges at higher elevations

Table 1
Summary of the indicative meanings used to estimate the relative elevation of the SLIPs and limiting points for the database. HAT-Highest Astronomical Tide; MHHW-Mean Higher High Water; MHW-Mean High Water; and MTL-Mean Tide Level.

Sample Type	Evidence	Reference Water Level	Indicative Range
Index Points			
Undifferentiated salt-marsh environment	Intertidal sediments with unnamed salt-marsh plant macrofossils or identification only to genus level (e.g., Shaw and Ceman, 1999; Gehrels et al., 2004; Daly et al., 2007; Shaw et al., 2010). Foraminiferal assemblages dominated by high and low marsh taxa (e.g., Scott and Greenberg, 1983; Scott et al., 1981, 1995; Gehrels et al., 2005; Barnett et al., 2016; Kemp et al., 2017).	(HAT to MTL)/2	HAT to MTL
Higher high marsh environment	Intertidal sediments with higher high marsh plant macrofossils (e.g. Shaw and Ceman, 1999; Shaw et al., 2010). Foraminiferal assemblages dominated by higher high marsh taxa (e.g., Shaw and Ceman, 1999; Barnett et al., 2016)	(HAT to MHHW)/2	HAT to MHHW
High marsh environment	Intertidal sediments with high marsh plant macrofossils (e.g. Shaw and Ceman, 1999; Gehrels et al., 2004; Daly et al., 2007; Shaw et al., 2010). Foraminiferal and diatom assemblages dominated by high marsh taxa (e.g., Scott and Greenberg, 1983; Scott et al., 1995; Gehrels et al., 2005; Barnett et al., 2016; Kemp et al., 2017)	(HAT to MHW)/2	HAT to MHW
Low marsh environment	In tertidal sediments with low marsh plant macrofossils (e.g. Shaw and Ceman, 1999; Patterson et al., 2004; Daly et al., 2007; Shaw et al., 2010). Foraminiferal assemblages dominated by low marsh taxa (e.g., Scott and Greenberg, 1983; Scott et al., 1981, 1995; Gehrels et al., 2005; Barnett et al., 2016; Kemp et al., 2017).	(MHW to MTL)/2	MHW to MTL
Shorre environment	Intertidal sediments with plant macrofossils and faunal assemblages typical of the *shorre* facies (e.g. Dionne, 1996, 1997; 1999; Dionne and Coll, 1995; Dionne et al., 2004).	(MTL to MLLW)/2	MTL to MLLW
Lower *shorre* to *slikke* environment	Intertidal sediments with plant macrofossils and faunal assemblages typical of the lower portion of the *shorre* facies and of the *slikke* facies (e.g. Dionne, 1996, 1997; 1999; Dionne and Coll, 1995; Dionne et al., 2004).	(MHW to MLLW)/2	MHW to MLLW
Slikke environment	Intertidal sediments with plant macrofossils and faunal assemblages typical of the *slikke* facies (e.g. Dionne, 1996, 1997; 1999; Dionne and Coll, 1995; Dionne et al., 2004).	(MTL to MLLW)/2	MTL to MLLW
Isolation Basin	Sediments recording the switch between freshwater and brackish/marine sediments that are supported by changing diatoms or macrofossil assemblages (e.g., Pienitz et al., 1991; Miousse et al., 2003; Glaser et al., 2004; Pendea et al., 2010).	(HAT to MTL)/2	HAT to MTL
Beach ridges	Gravelly to boulder beach deposits with macrofossil faunal assemblages dominated by *Mytilus edulis* shells (e.g., Allard and Tremblay, 1983; Lavoie et al., 2012; Tamura, 2012; Billy et al., 2015)	(3 + HAT to MLLW)/2	3 + HAT to MLLW
Beach deposits	Sandy to gravelly found mid to lower beach stratigraphic context (e.g., planar or cross-bedded lamination, e.g., Fraser et al., 2005; Lavoie et al., 2012) and with macrofossil faunal assemblages dominated by intertidal to shallow subtidal shells (e.g., *M. edulis*; *Mya arenaria*; *Nucella lapillus*, Matthiessen, 1960; Powers et al., 2006) or in-situ mussel banks of *M. edulis* shells.	(MHW to MLLW)/2	MHW to MLLW
Limiting Points			
Marine limiting	Identifiable in-situ marine shells found in marine and glacio-marine deposits (e.g., Hillaire-Marcel, 1976; Gray et al., 1993; Gray and Lauriol, 1985; Bell et al., 2005). Foraminiferal assemblages dominated by marine taxa (e.g., Cronin, 1979; Scott et al., 1987). Isolation basin sediments with marine diatoms and marine shell assemblages (e.g. Pienitz et al., 1991; Shaw et al., 2009).	MTL	Below MTL
Freshwater limiting	In-situ tree stumps (e.g., Catto et al., 2000; Dionne, 2001) Peat that does not meet the above requirements to be classified as an index point. Freshwater isolation basin sediments (lacustrine gyttja) dominated by freshwater diatoms and freshwater shells assemblages (e.g. Glaser et al., 2004; Pendea et al., 2010). Coastal archaeological settlements (e.g., Fitzhugh, 1977; Martindale et al., 2016)	MTL	Above MTL

(Otvos, 2000; Rovere et al., 2016). Therefore, we increased the indicative range to 3 m above HAT to MLLW (Table 1).

In our database, *M. edulis, Mya arenaria* and *Nucella lapillus* shells that were sampled in facies showing planar or cross-bedded lamination, suggesting deposition in lower beach deposits (e.g., Matthiessen, 1960; Svane and Ompi, 1993; Fraser et al., 2005; Powers et al., 2006), were assigned an indicative range of MHW to MLLW. We also applied this indicative range to three mussel banks sampled along the eastern Newfoundland coast (Grant, 1994; Bell et al., 2005). However, distribution of biological sea-level indicators may be affected by local variations in hydrodynamics and morphology (e.g. Rovere et al., 2015). For this reason, we added an environmental uncertainty of ± the tidal range (i.e., HAT-MLLW) to these SLIPs included in the database.

If a sea-level indicator formed in terrestrial (e.g., freshwater swamp or lakes) or marine environments (e.g., shoreface, prodelta, or glacio-marine sediments), we classified the sample as a limiting point (e.g., Shennan and Horton, 2002; Brooks and Edwards, 2006; Engelhart and Horton, 2012; Edwards et al., 2017). Terrestrial and marine limiting points have a lower and an upper limit of MTL, respectively. Therefore, reconstructed RSL must fall below terrestrial limiting points and above marine limiting points (Engelhart et al., 2015). Although these data cannot be used to produce SLIPs, they are important in understanding and interpreting RSL changes and constraining GIA models (e.g., Long et al., 2011; Vacchi et al., 2016; Khan et al., 2017).

Marine limiting dates were mainly from marine shells (e.g., *Mya truncata*, *Hiatella arctica, Ostrea* sp.) found in submarine and glacio-marine sedimentary facies (Hillaire-Marcel, 1976; Lauriol et al., 1979; Lavoie et al., 2012) and from coastal sediments with foraminiferal assemblages dominated by marine taxa (e.g., Cronin, 1979; Scott and Medioli, 1982, see details in Table 1).

Terrestrial limiting dates were from isolation basins dominated by terrestrial diatoms (e.g., Pienitz et al., 1991; Pendea et al., 2010) and archaeological sea-level indicators from the large number of prehistorical coastal settlements found along the eastern Canadian coast especially in Ungava Peninsula and Labrador (e.g. A Fitzhugh, 1977; Clark and Fitzhugh, 1990; Stopp, 1997; Martindale et al., 2016).

3.2. Tidal data

The tidal range is sensitive to the frequency of the astronomical forcing (i.e., the orbital configuration), ocean depth, density stratification, and coastal configuration, all of which have changed considerably since the LGM (Hill, 2016). Failing to account for a change in tidal-range would lead to a mis-estimation of the true magnitude of RSL change (Horton et al., 2013a). Notable tidal range changes have been reported for Nova Scotia and New Brunswick during the middle and late Holocene (Gehrels et al., 1995; Shaw et al., 2010).

To account for this possible effect in these regions, we predicted changes in tidal range using a nested modeling approach. Complete details of the approach taken here are available in Hill et al. (2011). Briefly, a global tidal model (Griffiths and Peltier, 2009), including self-attraction and loading, drag in shallow seas, and internal tide drag was first used to compute tidal constituent amplitudes and phases on a 800 × 800 regular grid. The results from the global model forced the open boundary of a regional tidal model spanning the western Atlantic Ocean, the Gulf of Mexico and the Caribbean Sea. The regional model (ADCIRC; Luettich et al., 1992) used an unstructured finite-element computational mesh to allow for very high resolution (1–2 km) at the shoreline. The tidal models do not include models of sediment infilling of either the estuaries and coastal lowlands or freshwater discharge from the catchments (Shennan et al., 2000).

We obtained modern tidal data using the Oregon tidal model (Egbert and Erofeeva, 2002). Following Hill et al. (2011) and Horton et al., (2013), we estimated paleo tidal data from the percentage change between the 0 ka and age of each SLIP, and applied that change to the modern datums collected using the OSU tidal model. Computational runs were carried out at 1 ka intervals from 10 ka to present. The geographical coverage of the model allowed the correction for palaeo-tidal range of 139 SLIPs from region 29, 30, 32, 33 and 34. No SLIPs older than 10 ka BP were present in these regions. For regions not covered by the Hill et al. (2011) tidal model (Newfoundland, St Lawrence corridor, Labrador, Ungava Peninsula and Hudson Bay) we extracted tidal data from the OSU tidal model, Admiralty tide tables (www.admiralty.co.uk) and from the Canadian Hydrographic service (waterlevels.gc.ca). These data, therefore, could not be corrected for paleotidal ranges at this time but could be modified appropriately if models become available in the future.

3.3. Vertical component and uncertainty of RSL

For each SLIP and limiting point, RSL is estimated using the following equation (Shennan and Horton, 2002):

$$RSL_i = A_i\text{-}I_i \quad (1)$$

where A_i is the altitude and I_i is the reference water level of sample *i*, both expressed relative to the same datum (MTL in our analyses.)

The total vertical uncertainty is obtained by adding in quadrature individual uncertainties according to Shennan and Horton (2002):

$$E_i = \left(e_{i,1}^2 + e_{i,2}^2 + \ldots + e_{i,n}^2\right)^{1/2} \quad (2)$$

where $e_1 \ldots e_n$ represent the sources of uncertainty for each SLIP and limiting point *i* including the indicative range and a number of additional uncertainties. They comprise an uncertainty associated with calculating the sample altitude. This can be as small as ±0.05 m with high precision surveying (e.g., Shennan, 1986), but the details on the surveying are often absent for data published prior to the 1980s and even for some later publications. For these samples, we adopted the height errors proposed by Peltier (1998) and Dyke and Peltier (2000), which are assumed to be ±0.5 m for samples at altitudes <10 m, ±5% of the altitude value between 10 and 50 m, and ±2.5% for altitudes >50 m.

For samples obtained by coring (e.g., salt-marsh samples), we included a core sampling uncertainty ranging from ±0.15 m for rotary coring and vibracoring to ±0.05 m for hand coring (Hijma et al., 2015). When available, the sample thickness is also incorporated into the vertical uncertainty term. We also calculated the angle of borehole uncertainty as a function of the overburden of the sample, taken in this study as 1% (Törnqvist et al., 2008). As stated in Section 3.2, we employed different sources to extract the tidal information in the regions included in the database. Thus, we further added a tidal uncertainty to our samples to account for any possible uncertainty related to the variability in the tidal information. This was quantified as 0.2 m for those regions in which tidal information was extracted from the OSU model and as 0.5 m for those regions for which tidal information was extracted from the coupled analysis of Admiralty and Canadian hydrographic services. These uncertainties derive from the cross comparison of the different available tidal datasets.

To account for sediment compaction, we subdivide SLIPs derived from the salt-marsh or intertidal sediments into basal and

intercalated categories (Horton and Shennan, 2009). Basal samples are those recovered from within the sedimentary unit that overlies the incompressible substrate and are considered to be virtually compaction-free (e.g., Goslin et al., 2015). Intercalated samples correspond to organic horizons in between clastic layers and, therefore, they are generally most prone to compaction (e.g., Hijma et al., 2015). Where stratigraphic information was unavailable for an index point, we conservatively interpreted it as intercalated. SLIPs from isolation basin and beach deposits are compaction-free.

3.4. Age component and uncertainty of RSL

In our database, ages of the SLIPs and limiting points were estimated using radiocarbon (^{14}C) dating of organic material from salt and freshwater marshes, marine and intertidal shells, as well as charcoal, wooden artefacts, bones and midden deposits from archaeological indicators.

Over 50% of the data points were collected between 1960 and 1989 CE. A notable concern with radiocarbon ages obtained during this period is the lack of a correction for isotopic fractionation (e.g., Törnqvist et al., 2015). This became a standard procedure at most laboratories by the late 1970s (Stuiver and Polach, 1977), but some laboratories have only started applying this correction since the mid-1980s (e.g., Hijma et al., 2015) with further confusions between uncorrected (analytical result) and conventional (corrected for isotopic fractionation, δ^{13}C) ages (Lavoie et al., 2012). The correction for isotopic fractionation is particularly important for marine shell samples, because it may produce errors of ~400 radiocarbon years (e.g., Lavoie et al., 2012; Törnqvist et al., 2015). We performed a correction for isotopic fractionation (e.g., normalized to −25‰ PDB), using the age correction and associated errors provided by Törnqvist et al. (2015) for a wide range of carbonaceous and calcareous material commonly used in sea-level studies. This normalization of the radiocarbon dataset benefited from and relied heavily on work by previous studies to validate the ^{14}C dataset along the Canadian coasts (e.g. Gray et al., 1993; Dyke and Peltier, 2000; Dyke, 2004; Bell et al., 2003; McNeely and Brennan, 2005; Lavoie et al., 2012, Martindale et al., 2016, among others). These publications identified and corrected the erroneous calibrations and mistakes in transcription found in second and third hand literature producing a dataset of conventional radiocarbon dates. However, for many samples listed with BGS, QU, UL and UQ Lab codes (see Appendix A) and dated between the mid-1970s and the mid-1990s, it was very complex to access the original protocol. Following Dyke and Peltier (2000) and Dyke (2004), we assumed they were not normalized to −25‰ PDB. 118 of these samples were crucial to reconstruct the RSL evolution in the St. Lawrence corridor (regions 21 to 24), notably in the early to mid-Holocene period. Due to the uncertainty in the normalization process, the RSL records based on these samples should be used with caution.

An additional problem is related to the radiocarbon dating of deposit-feeding marine molluscs from calcareous sediments in eastern Canada. Several of these samples yielded greater apparent radiocarbon ages than do suspension feeders (e.g., Dyke et al., 2002; McNeely et al., 2006; England et al., 2013). This raises issues about the accuracy of dates on deposit feeders from calcareous terrains, which has led to the exclusion of these data in recent syntheses of deglaciation both in Canada and Greenland (e.g., Dyke, 2004; England et al., 2006). For this reason, these samples (less than the 3% of the radiocarbon dates) were included in the database but not used for the RSL reconstructions.

We calibrated the normalized ages to sidereal years using CALIB 7.1 (Stuiver et al., 2017). We used a laboratory multiplier of 1 with 95% confidence limits and employed the IntCal13 and Marine13 (Reimer et al., 2013) datasets for terrestrial samples and marine samples, respectively. Information on the necessary reservoir correction was taken from the Marine Reservoir Database (Reimer and Reimer, 2001), mainly based on the extensive dataset provided by McNeely et al. (2006) and Coulthard et al. (2010).

All RSL data points are presented as calibrated years before present, where year 0 is 1950 CE (Stuiver and Polach, 1977).

4. Spatio-temporal statistical model of postglacial RSL changes

We constructed a spatio-temporal empirical hierarchical model (EST-GP) to reconstruct magnitudes and rates of RSL change (with associated uncertainty) from SLIPs along the eastern Canadian coastline. This analysis was restricted to the Holocene period because most SLIPs come from this time period (see section 6), with earlier times dominated by limiting data. Similar models have recently been used to estimate the common global sea-level signal over the Common Era (Kopp et al., 2016), as well as to reconstruct regional sea-level changes in a variety of areas over the Holocene and Last Interglacial (e.g., Kopp et al., 2009; Khan et al., 2017). Ashe et al. (this issue) provide a more comprehensive discussion.

As a hierarchical model, an EST-GP distinguishes between uncertainty that arises at the data level, for example, due to measurement uncertainty or proxy interpretation uncertainty, and uncertainty that arises at the process level, due to spatial and temporal variability in sea level itself. As a spatio-temporal model, it leverages the correlation structure of the sea-level field; for example, it recognizes that an observation associated with a single point in space and time is informative about sea level at proximal locations and times. Thus, it can estimate RSL for locations and times where there are no direct observations. We employ it to reconstruct the spatio-temporal field of RSL for 10,000 km of Canadian coastline from 12 to 0 ka BP. Rates of RSL change (and their uncertainties) are calculated through a linear transformation of the RSL predictions.

4.1. Data level

At the data level, the EST-GP models the noisy process of observing the spatio-temporal sea-level field. Each SLIP$_i$ (information provided by limiting points is not modeled) provides a noisy measure, y_i, of the sea-level field, $f(\mathbf{x}_i, t_i)$ at geographic location $\mathbf{x}_i$ and true (noise-free) age t_i. The true age t_i of each observation is also uncertain; we have a noisy observation of age, $\widehat{t_i}$.

$$y_i = f(\mathbf{x}_i, t_i) + \varepsilon_i^y$$

$$\widehat{t_i} = t_i + \varepsilon_i^t$$

Here, $\widehat{t_i}$ are the midpoints of calibrated ages; ε_i^y are the uncertainties in the vertical component RSL; and ε_i^t are errors in age. The RSL uncertainties are treated as uncorrelated and normally distributed. The geochronological uncertainties are incorporated using the noisy-input Gaussian Process (NIGP) method of McHutchon and Rasmussen (2011).

4.2. Process level

The process level models the unobserved sea-level field over space and time. It represents the field as the sum of three sub-fields, each of which has its own distinct prior expectations regarding spatial and temporal scales of variability:

$$f(\mathbf{x},t) = c(t) + r(\mathbf{x},t) + l(\mathbf{x},t) + w(\mathbf{x},t)$$

The common signal, $c(t)$, is the same throughout the Eastern Canada domain, while the regional signal, $r(\mathbf{x}, t)$, is spatially correlated but varies through the domain. The local signal, $l(\mathbf{x},t)$, is assumed to be independent at each spatial point. A spatially uncorrelated white-noise term $w(\mathbf{x}, t)$, captures high-frequency variability.

Each term in $f(\mathbf{x},t)$ has a Gaussian process (GP) prior (Rasmussen and Williams, 2006). Each GP prior is defined by a mean function, which expresses prior expectations regarding the mean value of the term at each point in space and time, and a covariance function, which expresses prior expectation about the variance of each point and covariance between points. All of the terms except $r(\mathbf{x},t)$ have a zero-mean prior. The prior mean function for the regional sub-field, $r(\mathbf{x},t)$, is the GIA curve predicted by Peltier et al. (2015) at each location. Effectively, we removed the GIA model predictions, fit the EST-GP (with zero-mean priors) to the mismatch between the observations and the GIA predictions, and then add back in the GIA predictions.

4.3. Hyperparameter level

The hyperparameter level of the EST-GP represents key parameters for the priors in the process level. These include prior expectations about the variance and the spatial and temporal scales of variability of the different terms in equation (3). As an empirical model, the EST-GP employs point estimates of these hyperparameters. The point estimates are optimized to maximize the likelihood of the model given the observations. Details on the optimized hyperparameters employed in this study are provided in Appendix B.

5. The new database of postglacial RSL changes along the eastern Canadian coastline

We reconstructed the RSL history of 34 regions of eastern Canada using a database composed of 405 SLIPs and 687 limiting points (Appendix A, Fig. 2A and B). Spatially, RSL reconstructions covered most of Newfoundland, Nova Scotia, New Brunswick, and the St Lawrence corridor. At the highest latitudes, the RSL reconstructions are characterized by a significant decrease in the number of SLIPs and are often based only on limiting points, especially along the Ungava Peninsula and Labrador coasts. The age range of the data spans the last ~16 ka. However, with the exception of one sample from Newfoundland, the temporal span of SLIPs is restricted to the Holocene period (last ~12 ka), with a general increase in their number throughout the Holocene (Fig. 2B). Compaction-free SLIPs (e.g., isolation basins and beach deposits) and basal SLIPs (minimally affected by compaction) represent ~26% and ~23% of the database, respectively (Fig. 2B).

Our database updated previous regional compilations (e.g., Dionne and Coll, 1995; Peltier, 1998; Mitrovica et al., 2000; Dyke and Peltier, 2000; Dyke, 2004; Bell et al., 2003; Gehrels et al., 2004; Shaw et al., 2010; Lavoie et al., 2012; Simon et al., 2016). For example, we increased the number of SLIPS and limiting data compared to the database produced by Peltier (1998) for southeastern Hudson Bay (Fig. 3; regions 3, 4 and 5). The new database contains 37 SLIPS and 110 limiting points compared to the 71 limiting points in Peltier (1998). The production of a number of SLIPs in the new database is due to both the addition of new data (e.g., Glaser et al., 2004; Pendea et al., 2010; Lavoie et al., 2012) and the reinterpretation of 11 limiting dates as SLIPs on the basis of our new indicative meanings (see section 3.1).

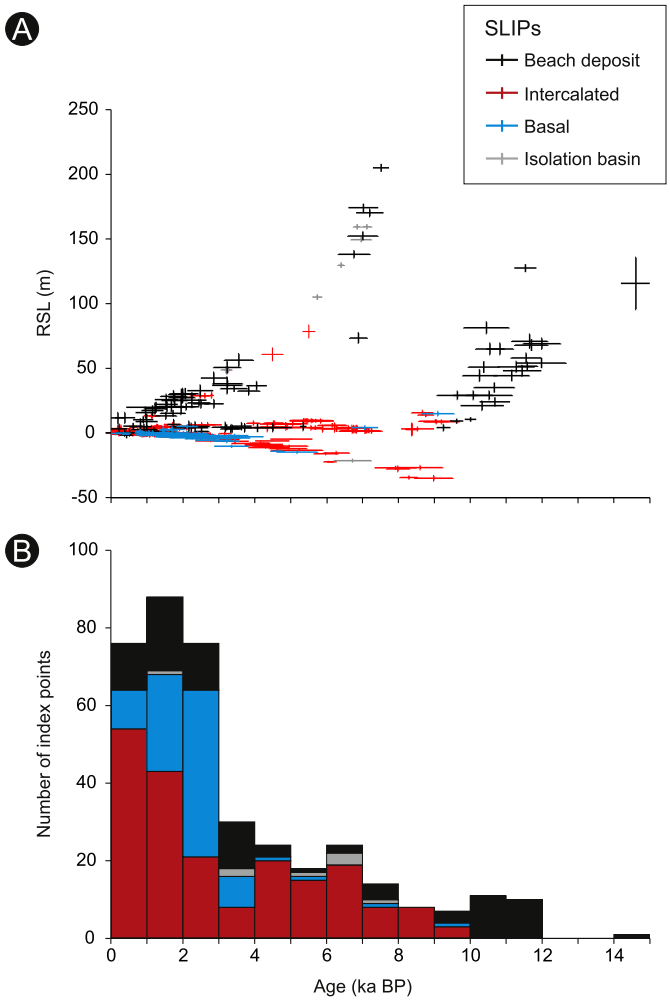

Fig. 2. (A) Plot of all validated sea-level index points (SLIPs). (B) Stacked histogram of the validated SLIPs (definitions and criteria for validated points are explained in the text) collected along the eastern Canadian coastline.

Furthermore, our correction for palaeo-tides improved the quality of SLIPs in the Bay of Fundy (regions 29, 33 and 34) and along a significant portion of outer Nova Scotia (regions 30 and 32). Unfortunately, this correction was not possible for the remaining coastal regions included in the database due to the geographical extent of the palaeo-tidal model (see section 3.2). For this reason, it is presently impossible to quantify any possible RSL change related to changes in the tidal ranges along the Holocene for a large sector of the eastern Canadian coastline. Tidal amplification would have potentially had a significant role in controlling the RSL changes, for instance in the inner portion St. Lawrence corridor, where GT values presently exceed ~5.5 m. Future development of the palaeo-tidal model (Hill et al., 2011) at higher latitudes will help to address these issues.

In some coastal regions, such as in the Hudson Bay, and partly in the St Lawrence corridor, we predominantly have to use marine shells to produce SLIPs. Given ongoing issues with interpreting marine reservoir effects, these may be less reliable than terrestrial-based samples that were largely used to produce SLIPs in New Brunswick and Nova Scotia and along much of the Newfoundland coast.

All of the eastern Canada SLIPs define three main RSL patterns (Fig. 2 A) that can be summarized by the following three GIA-related categories:

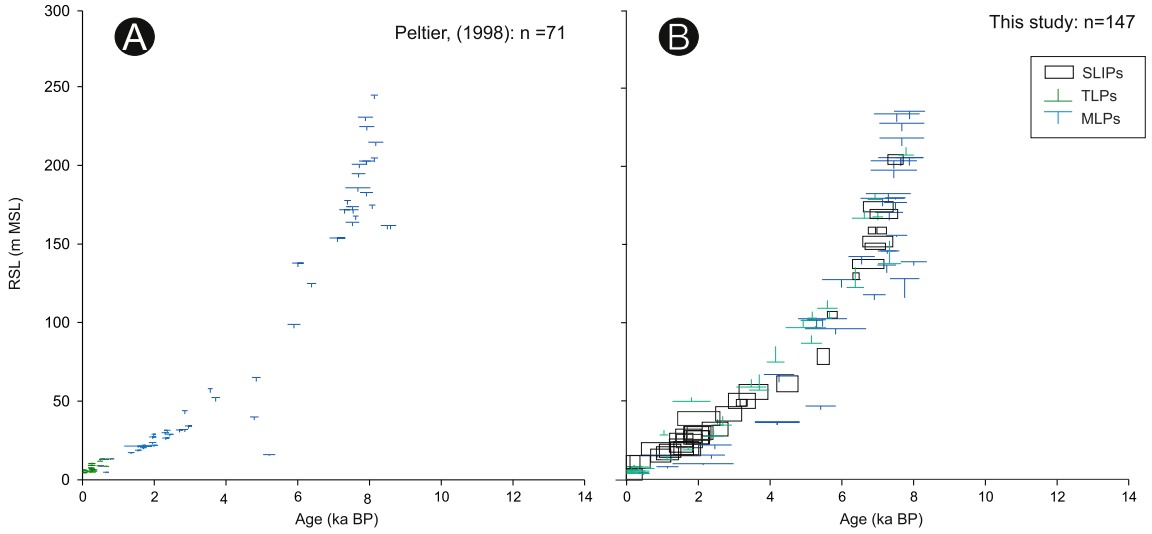

Fig. 3. Comparison between the RSL history in the southeastern portion of Hudson Bay (regions 3, 4 and 5) reconstructed by Peltier (1998) and in the present study (B). SLIPs are Sea-Level Index Points, TLPs are Terrestrial Limiting Points and MLPs are Marine Limiting Points.

i) Uplifting regions (including Hudson Bay, Ungava Peninsula and Labrador regions as well as the northwestern part of Newfoundland) where a continuous RSL fall is recorded.
ii) Transitional regions (including the St Lawrence corridor regions, much of Newfoundland as well as the New Brunswick and western Nova Scotia coasts) record a composite and non-monotonic RSL pattern. This consists of a late Pleistocene to early-Holocene RSL drop to a spatially variable lowstand followed by continuous RSL rise (Newfoundland, New Brunswick and western Nova Scotia regions) or by the establishment of a mid-Holocene RSL highstand and a subsequent drop to the present RSL (St Lawrence corridor regions).
iii) Subsiding regions (eastern Nova Scotia regions) where a continuous RSL rise is recorded during the entire Holocene.

5.1. Uplifting regions

The most complete and representative RSL records for this type of coast were found in SE Hudson Bay (regions 4 and 5, Fig. 4, SLIPs n = 34; limiting points n = 97). Here, a wide range of sea-level indicators (e.g., raised beaches, marine and intertidal deposits, isolation basins; Hardy, 1976; Allard and Tremblay, 1983; Barber et al., 1999, Pendea et al., 2010; Lavoie et al., 2012) were used to infer the postglacial RSL evolution, which covers the last ~8.5 ka. At 7.5 ± 0.2 ka, an index point places RSL at 205 ± 3 m, in agreement with a suite of marine limiting points documenting the progressive drop of the RSL from ~289 m at 8.5 ± 0.6 ka to ~177 m at 7.1 ± 0.6 ka. A suite of SLIPs and limiting points constrain well the RSL evolution between ~7.1 and ~6.8 ka with a progressive drop from 170 ± 3 to 138 ± 3 m. Younger SLIPs well document the RSL evolution in the mid to late Holocene transition. RSL was 130 ± 2 m at 6.4 ± 0.1 ka and ~105 ± 2 m at 5.7 ± 0.1 ka. In the late Holocene, RSL is very well constrained by both SLIPs and limiting points. They document the progressive RSL fall from 56 ± 5 m at 3.5 ± 0.4 ka to ~30 ± 4 m at 1.9 ± 0.4 ka and finally to the present datum. The RSL variation in the last 1.0 ka was within ~20 m.

The continuous RSL fall is clearly recorded also in the remaining Hudson Bay regions (Fig. 4, regions 1, 2, 3, 6, 7, SLIPs n = 27; limiting points n = 86) and along the Ungava Peninsula (Fig. 5, regions 8, 9, 10, 11, SLIPs n = 3; limiting points n = 84). Similarly to the previous regions, RSL data were mainly derived from raised beach, marine and intertidal deposits and isolation basins (e.g., Matthews, 1966; Gray et al., 1993; Lemieux et al., 2011; Simon et al., 2014).

Spatial variability exists across the uplifting regions due to the variations in local ice load history (Roy and Peltier, 2015; Simon et al., 2016). The lack of SLIPs along much of the Ungava peninsula did not allow a strong constraint on this spatial variability. The sole exception is represented by the southern Ungava Bay region (11, Fig. 5), where a suite of SLIPs is available. These data show that, in the second part of mid-Holocene (5.6 ± 0.3 ka) RSL in southern Ungava Bay was ~100 m lower than near the centre of the former ice-sheet (i.e., regions 4 and 5).

Along the Labrador coast (Fig. 6, regions 12 to 15, limiting points n = 61) the RSL record is poor and only constrained by limiting points spanning the last ~10.0 ka (Fig. 5). Limiting data are mainly derived from raised marine deposits and archaeological evidence of coastal settlements (e.g. Clark and Fitzhugh, 1990; Stopp, 1997 Martindale et al., 2016). These data suggest a continuous RSL drop for the whole Holocene but do not significantly improve the previous compilations (e.g. Clark and Fitzhugh, 1990) due to the lack of robust SLIPs.

The northwestern portion of Newfoundland differs from the rest of Newfoundland (above ~50° N see section 5.1, region 16, Fig. 6) and can be classified as uplifting coast. Here, RSL remained always above the present MSL in the last ~16 ka. A suite of SLIPs and terrestrial limiting points robustly constrains the RSL evolution in the mid to Late Holocene where RSL dropped from 4.9 ± 3.2 m at ~5.3 ka to 2.4 ± 2.2 m at ~1.7 ka and finally to the present MSL at ~1.2 ka. This region, located more than 1300 km away from the centre of the Quebec/Labrador ice-sheet represents the most distant eastern Canadian coastal sector showing evidence of continuous GIA-related RSL fall since the last glaciation.

5.2. Transitional regions

The dataset from the Newfoundland coast (Fig. 7, regions 16 to 20, SLIPs n = 46; limiting points n = 114) confirms the transitional nature of this island from a GIA perspective. The new dataset of SLIPs spanning the last ~16.0 ka produced using raised beaches and intertidal deposits (mainly salt-marsh peats), updated the previous

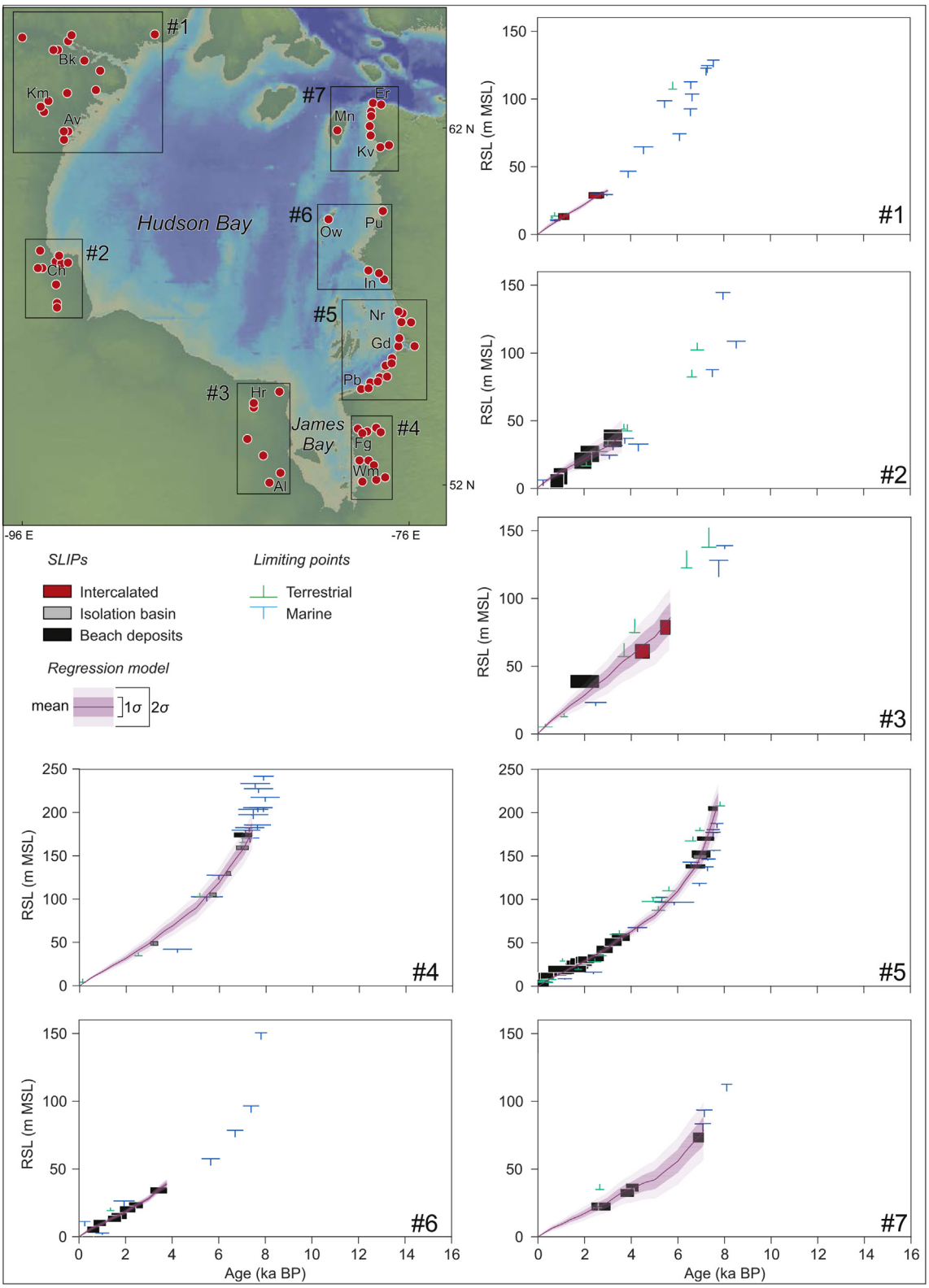

Fig. 4. RSL reconstructions and spatio-temporal statistical model predictions in the Hudson Bay (regions 1 to 7). SLIPs (boxes) are plotted as change in sea level relative to present against calibrated age. Limiting points are plotted as terrestrial or marine horizontal lines. Dimensions of boxes and lines for each point based on 2σ elevation and age uncertainties. Predictions are not shown for a region before the earliest SLIP in the region. Red dots indicate the position of the cluster of samples used to compile the database in every region. Bk is Baker lake, Av is Arviat, Ch is Churchill, Hr is Cape Henrietta, Al is Albany River, Wm is Wemindjii, Fg is Fort George, Pb is Petite Riviere de la Baleine, Gd is Umiujaq/Lac Guillaume-Delisle, Nr is Nastapoka river, In is Inukjuak, Ow is Ottawa Islands, Pu is Povungnituk, Kv is Kovik Bay, Mn is Mansell Island, Er is Erik cove. (For interpretation of the references to colour in this figure legend, the reader is referred to the Web version of this article.)

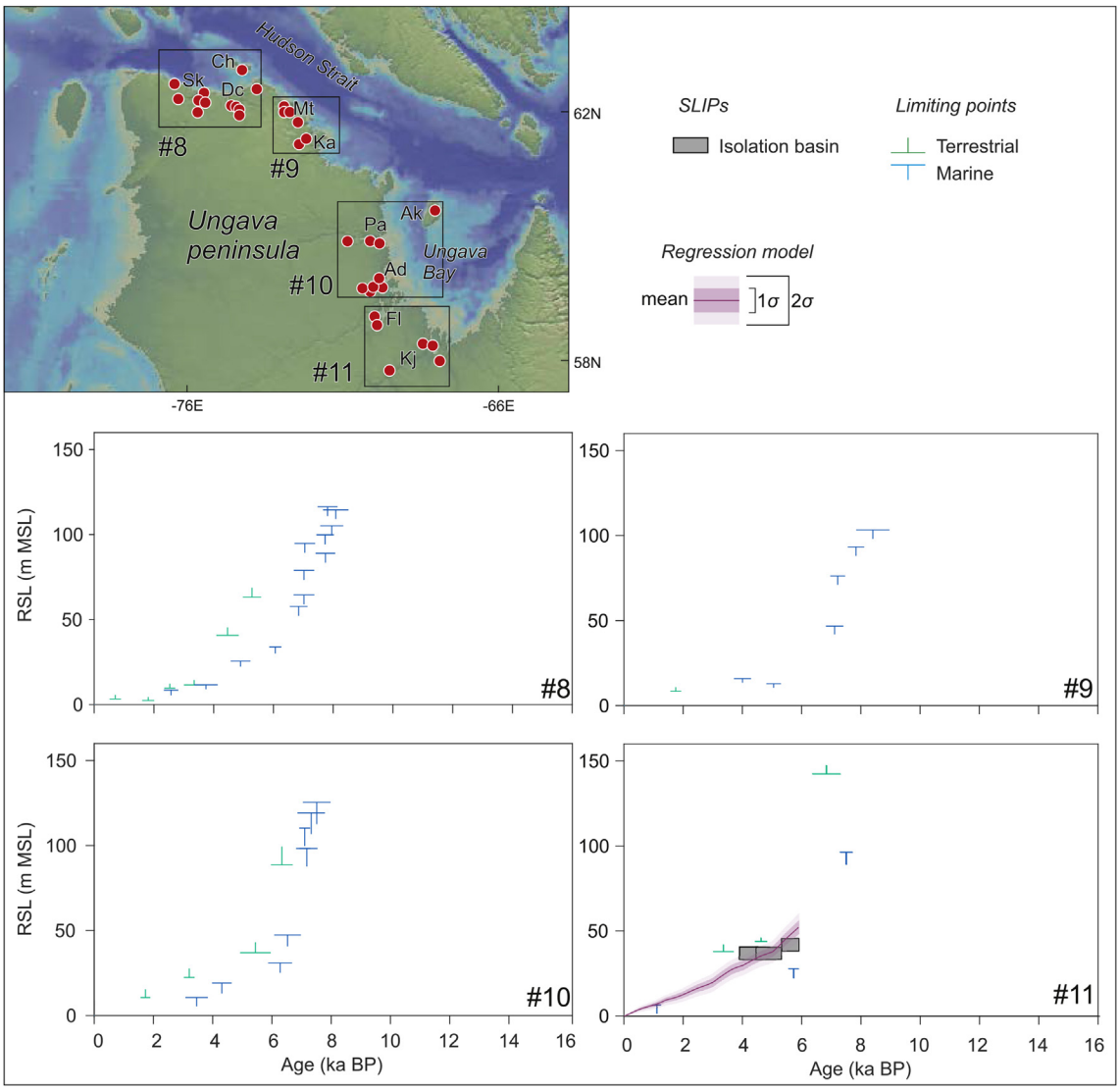

Fig. 5. RSL reconstructions and spatio-temporal statistical model predictions in the Ungava Peninsula (regions 8 to 11), plotted as in Fig. 4. Sg is Sugluk, Dc is Deception Bay, Ch is Charles Island, Mt is Cap Martigny, Ka is Kangiqsujuaq-Wakeham Bay, Ak is Akpatok Island, Pa is Payne Bay, Ad is Hope's Advance Bay, Fl is Baie aux Feuilles and Kj is Kuujjuaq.

regional compilations (e.g., Shaw and Forbes, 1995; Bell et al., 2003, 2005; Daly et al., 2007) with new data (e.g., Kemp et al., 2017) and the standardization of the SLIPs according to the procedure described in section 3. The RSL histories show variability along the Newfoundland coast, supporting the previously-identified major change in the pattern of GIA at ~50° N (Liverman, 1994; Bell et al., 2003; Daly et al., 2007).

In regions 17, 18, 19 and 20 (Fig. 7), located below the ~50° N boundary, our data are consistent with an early-Holocene rapid drop to a RSL lowstand (Shaw and Forbes, 1995; Shaw and Potter, 2015). However, the mid-Holocene RSL record, composed only of limiting points, did not provide new insights into depth, chronology and spatial variability of the lowstand with respect to the previously available literature (e.g. Shaw and Forbes, 1995; Shaw et al., 2006; Shaw and Potter, 2015). Grant (1980, 1989) considered the eastern Newfoundland sector (19) as the only region of the island showing a continuous postglacial RSL rise. However, a number of raised beaches and marine deposits were identified in this region at elevation ranging up to ~15 m (Rogerson and Tucker, 1972; Tucker et al., 1982; Catto and Taylor, 1998; Catto et al., 2000; Dyke et al., 2005), which may challenge the hypothesis of a continuous postglacial RSL rise. These paleo shorelines cannot be included in the database due to the absence of radiocarbon dates on these deposits (Batterson and Taylor, 2003), and our record, based on the available radiocarbon data, is not sufficiently robust to solve this issue. Marine limiting points only constrain the RSL above ~ −33 m in the last ~10.6 ka and above ~ −26 m in the last ~7.4 ka. In the late Holocene, a suite of SLIPs indicate there was ~1.4 m of RSL rise in the last 2.1 ± 0.3 ka.

Our database documents the variability in the late Holocene records across Newfoundland. A suite of SLIPs indicates ~2.4 m of RSL rise in the last 2.7 ± 0.2 ka for southwestern Newfoundland (region 18), ~1.4 m of RSL rise in the last 2.1 ± 0.2 ka for eastern Newfoundland (region 19), and stability close to present RSL during the last ~3.0 ka for mid-western (17) and northeastern Newfoundland (20). This further underlines the importance of Newfoundland, where the migration of the forebulge from southeast to northwest across the island resulted in a great variability in postglacial sea-level curves ranging from a subsiding coast in the southeast to an uplifting coast in the northwest (Daly et al., 2007; Shaw and Potter, 2015).

As stated above, the other key transitional zone is represented

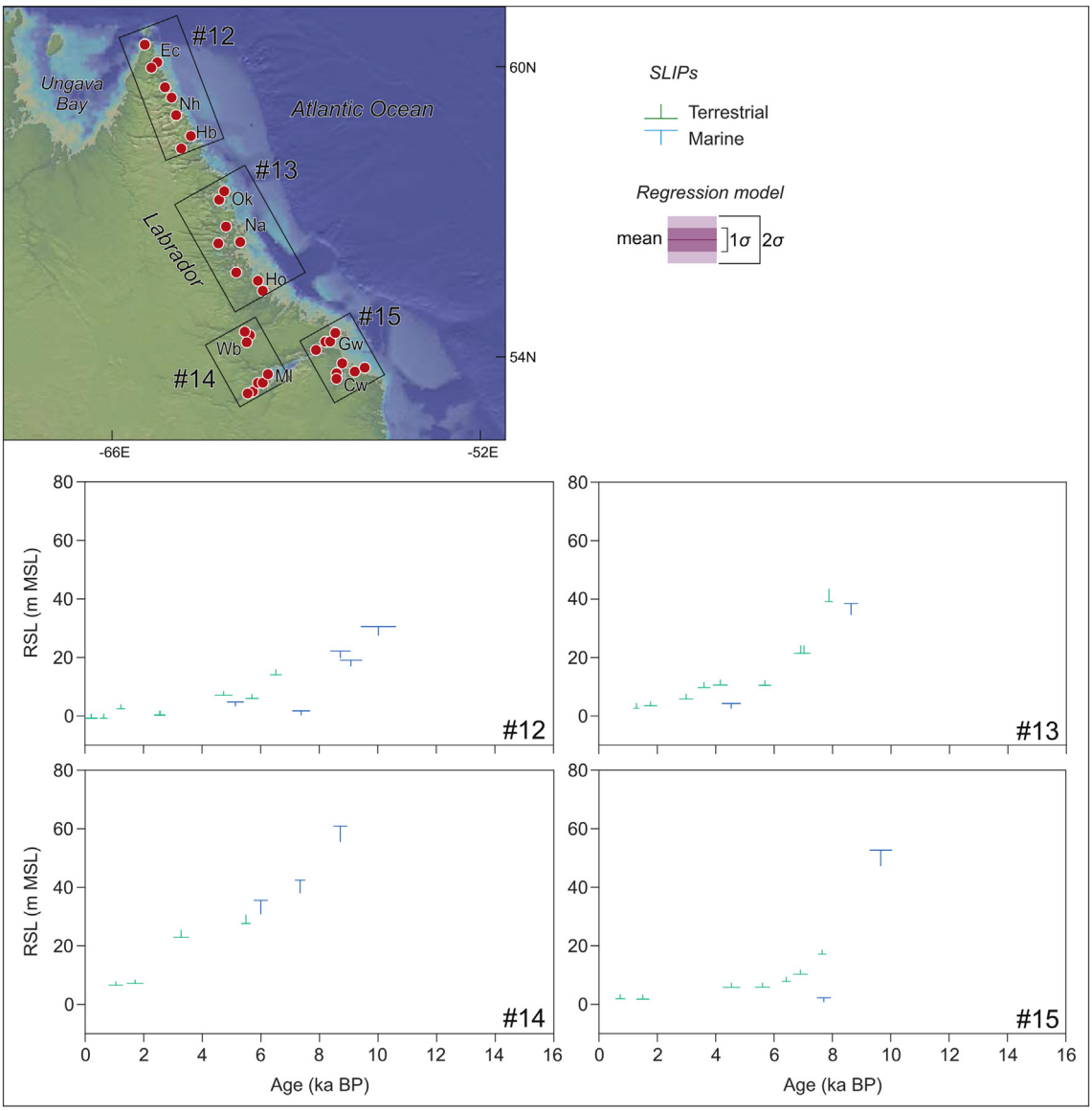

Fig. 6. RSL reconstructions and spatio-temporal statistical model predictions in Labrador (regions 12 to 15), plotted as in Fig. 4. Ec is Eclipse Fiord, Nh is Nachvak Fiord, Hb is Hebron Fiord, Ok is Okak islands, Na is Nain, Ho is Hopedale, Wb is White Bear Lake, Ml is Melville lake, Gw is Groswater Bay and Cw is Cartwright.

by the St. Lawrence corridor. Here, both GPS and tidal gauge data identify a major hinge line between regions currently experiencing RSL rise and fall from GIA (e.g. Sella et al., 2007; Argus and Peltier, 2010; Peltier et al., 2015; Roy and Peltier, 2017). Our database (Fig. 8, region 21 to 24, SLIPs n = 124; limiting points n = 118) represents an important tool to analyse the RSL evolution in this crucial sector of the Canadian coast. RSL reconstructions span the last ~15.0 ka and SLIPs were produced using beach deposits and intertidal sediments (salt-marsh peats and samples found in *slikke* and *shorre* facies, Dionne, 1990; Dionne and Coll, 1995, see section 3.1). It is important to note that difficulties in accessing the original radiocarbon protocols of early to mid-Holocene marine shell samples used to produce SLIPs and limiting points in the St. Lawrence corridor reduced the age reliability of these samples (see section 3.4). The RSL histories from this coastal sector show a uniform pattern. RSL fell rapidly near the present MSL in early-Holocene followed by a mid-Holocene highstand that was generally within ~10 m MSL. This variability in the temporal pattern of RSL change reflects the changing influence of GIA and the interplay with fluctuating rates of global meltwater inputs (e.g. Peltier, 2002; Milne et al., 2005; Peltier and Fairbanks, 2006). The RSL highstand recorded in the St Lawrence corridor spans almost the entire mid–Holocene with maximum elevations observed at ~5.5 ka. The timing of the highstand is comparable (within errors of ± ~0.5 ka) to those recorded at the periphery of the Cordilleran ice-sheet in southwestern Canada (Engelhart et al., 2015) and the British Ice-sheet in northeastern Scotland (Shennan et al., 2000). The global distribution of this highstand at transitional regions may suggest a global control, most likely related to the reduction of the meltwater input at ~7 ka caused by the final melting of the Laurentide ice-sheet (Carlson et al., 2008; Ullman et al., 2016). This resulted in isostasy (ongoing slow uplift at the regions under discussion) becoming the dominant process in controlling the evolution of RSL. This switch results initially in a stillstand in RSL as global meltwater input and land uplift balance each other before a fall from the mid-Holocene highstand to present MSL when there is a further decrease in the meltwater input after ~4 ka (Peltier, 2004; Milne et al., 2005; Engelhart et al., 2009) and land uplift now occurs at

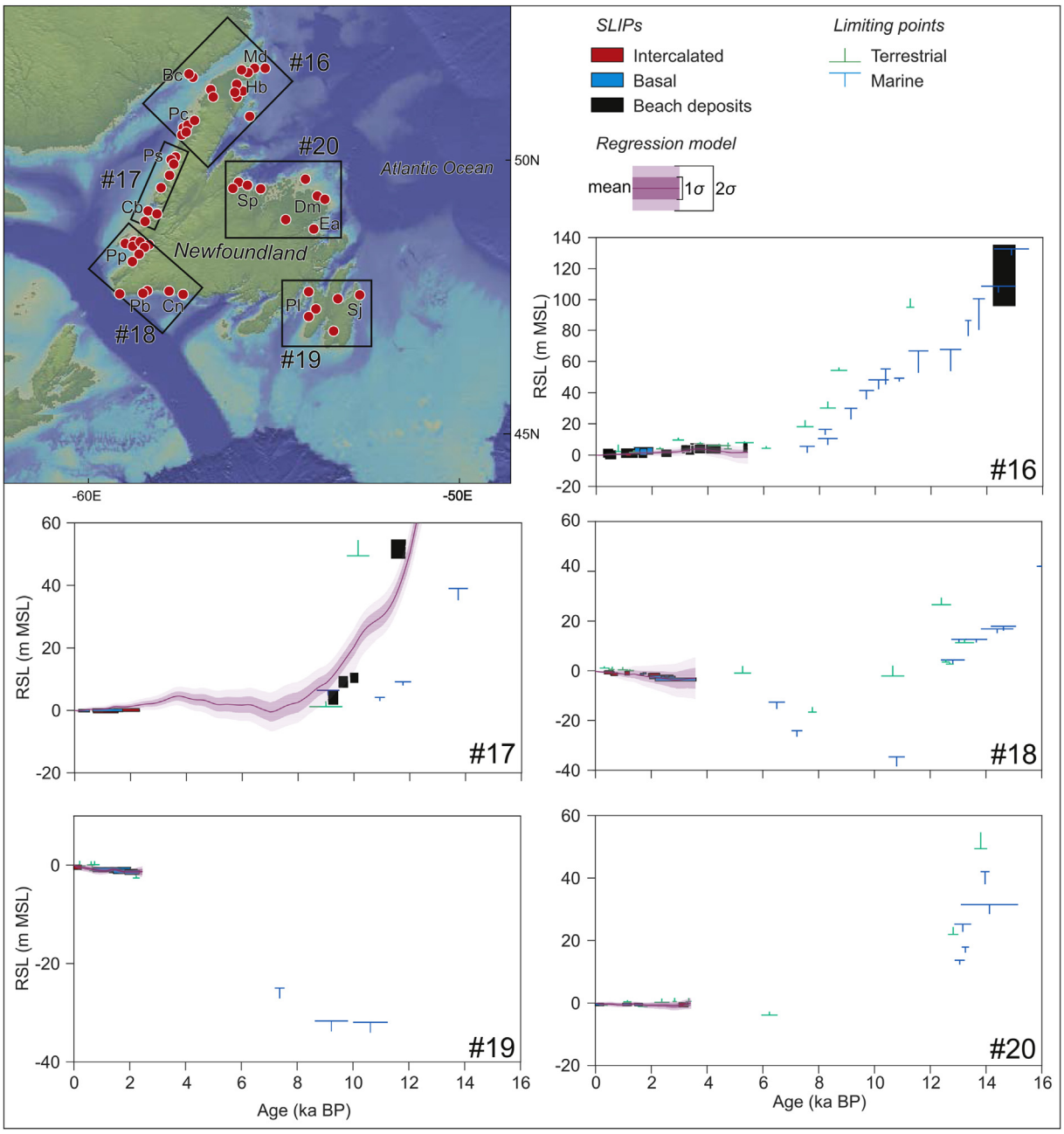

Fig. 7. RSL reconstructions and spatio-temporal statistical model predictions in Newfoundland (regions 16 to 20), plotted as in Fig. 4. Md is Anse aux meadows, Hb is Hare Bay, Bc is Blanc Sablon, Pc is Port au choix, Ps is St. Pauls inlet, Cb is Corner brook inlet, Pp is Port au port, Pb is Port aux basques, Cn is Connoire Bay, Pl is Placentia bay, Sj is Saint John's, Ea is Eastport, Dm is Deadman's Bay and Sp is Springdale.

a greater rate than meltwater input. The quality of the SLIPs included in the database precludes us from precisely constraining the variability in highstand elevation along the St. Lawrence corridor. Similarly, we presently cannot assess any possible tectonic influence of the RSL changes within the Charlevoix Seismic Zone (CSZ, region 24). This is mainly related to the large vertical uncertainty bars of the SLIPs in these regions that would be significantly improved by the development of a regional predictive plant zonation- and/or microfossil-based transfer functions (e.g., Gehrels, 2000; Kemp and Telford, 2015; Barnett et al., 2016) that are presently not reported in the St Lawrence estuary. Future high-resolution mid to late-Holocene RSL reconstructions are much needed for this area which represents a key transitional area in the isostatic pattern along the eastern Canadian coast. The broad elevational ranges suggested by this dataset could provide a roadmap to target suitable areas for high-resolution studies.

Lastly, a non-monotonic postglacial evolution also characterized the New Brunswick and eastern Nova Scotia regions (Fig. 9, region 25 to 27 and Fig. 10, regions 29, 33 and 34; SLIPs n = 129; limiting points n = 85. In these regions, RSL dropped to a lowstand in the late Pleistocene with a continuously rising RSL during the Holocene. The absolute magnitude of the lowstand is difficult to quantify due to the absence of robust SLIPs in these regions. However, a marine limiting point collected in eastern Northumberland Strait (Kranck, 1972) constrains RSL above ~ −35 m at the late-Pleistocene/early-Holocene transition (Fig. 9, region 27). Absence

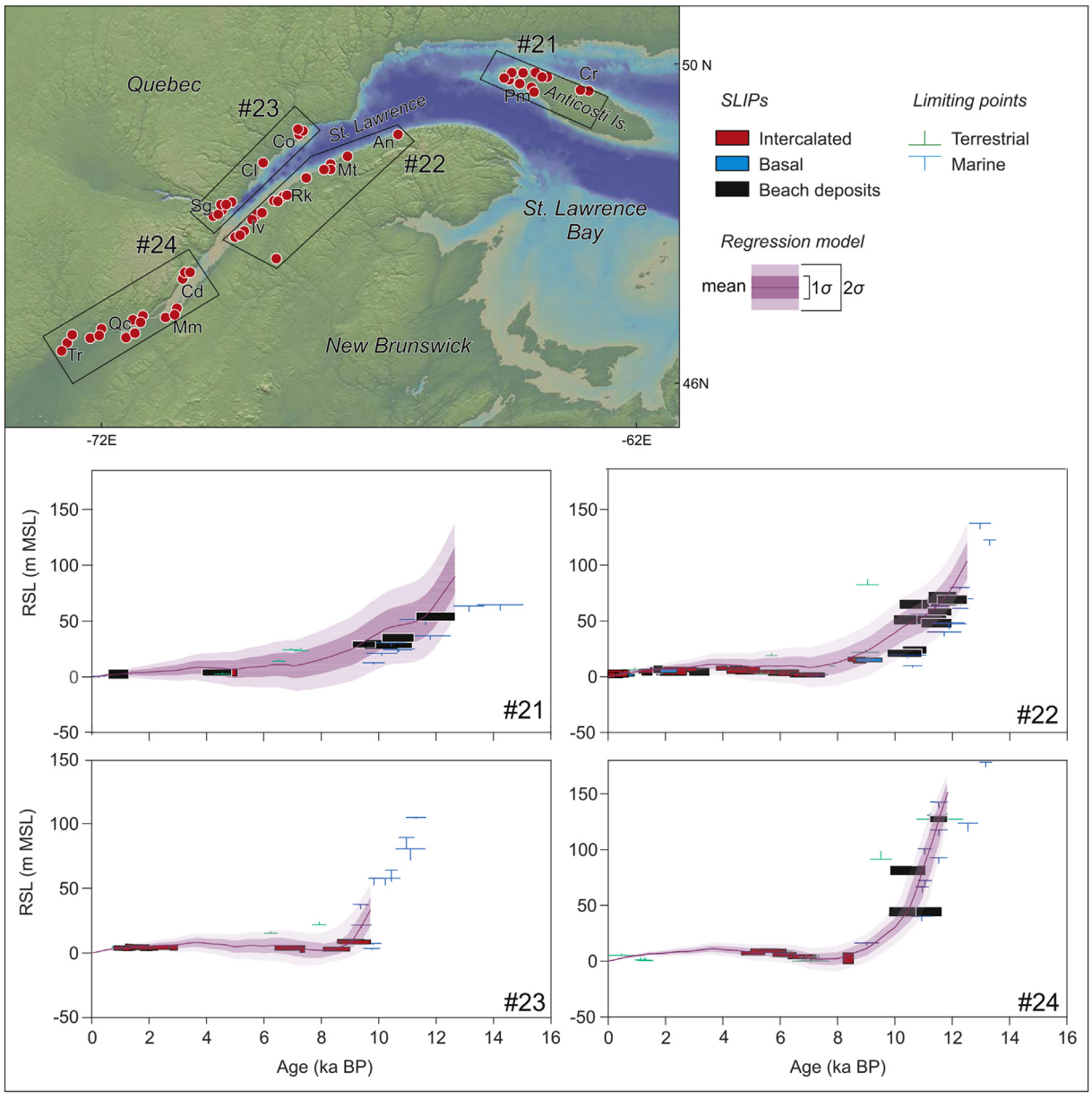

Fig. 8. RSL reconstructions and spatio-temporal statistical model predictions in the St. Lawrence corridor (regions 21 to 24), plotted as in Fig. 4. Pm is Port Menier, Cr is Pointe Carleton, An is Ste-Anne-des-Monts, Mt is Matane, Rk is Rimouski, Iv is Ile Verte, Co is Baie Comeau, Cl is Cap Colombier, Sg is Saguenay Fiord, Cd is Ile aux Coudres, Mm is Montmagny, Qc is Quebec City and Tr is Trois rivieres.

of data prohibits robustly quantifying the depth of the lowstand in the northern Bay of Fundy. In this region, the oldest SLIP documents ~28 m of RSL rise since the beginning of mid-Holocene (8.0 ± 0.3 ka, Fig. 10, region 29). Since ~5.0 ka BP, a large increase in tidal range (~20%, Shaw et al., 2010) played a major role in controlling the RSL evolution, most notably in the northern Bay of Fundy (e.g., Gehrels et al., 1995; Shaw et al., 2010). SLIPs and limiting points are partly contrasting between ~5.0 and ~4.0 ka. This is not surprising because variability in the timing of the tidal expansion is reported to have created disparities in the RSL evolution among sites, notably between ~5.0 and ~3.0 ka (Shaw et al., 2010). However, a robust record of younger SLIPs is consistent with a RSL placed at ~ -3.1 m at ~3.3 ka followed by a rise to present at ~2.0 ka.

Recent investigations performed in the Magdalen Islands archipelago (region 26, Fig. 9) provided insights into the RSL changes in a previously poorly-studied portion of the Canadian coast (Barnett et al., 2017; Rémillard et al., 2017). A series of recent OSL dates on subtidal deposits (Rémillard et al., 2017) suggests that RSL was above present until ~11 ka. Terrestrial limiting points (region 26, Fig. 9) indicate that, at 10.8 ± 0.2 ka, RSL had dropped below the present. Furthermore, Rémillard et al., (2016, 2017) reported that an organic horizon containing leaves and tree trunks found at ~ −17 m yielded an age of ~9.8 ka. However, this sample is excluded from the database because the original radiocarbon age was not reported and so could not be calibrated. In Magdalen Islands, SLIPs are restricted to a short period during late-Holocene. They indicate that the entire RSL variation in the last 1.3 ± 0.02 ka was within ~1.5 m. This record is of importance to better constrain the GIA related subsidence off the New Brunswick coast. These studies improved on the previously available data that were mostly collected in Prince Edward Island (region 27, Fig. 9) more than 30 years ago (Scott et al., 1981) with large age errors.

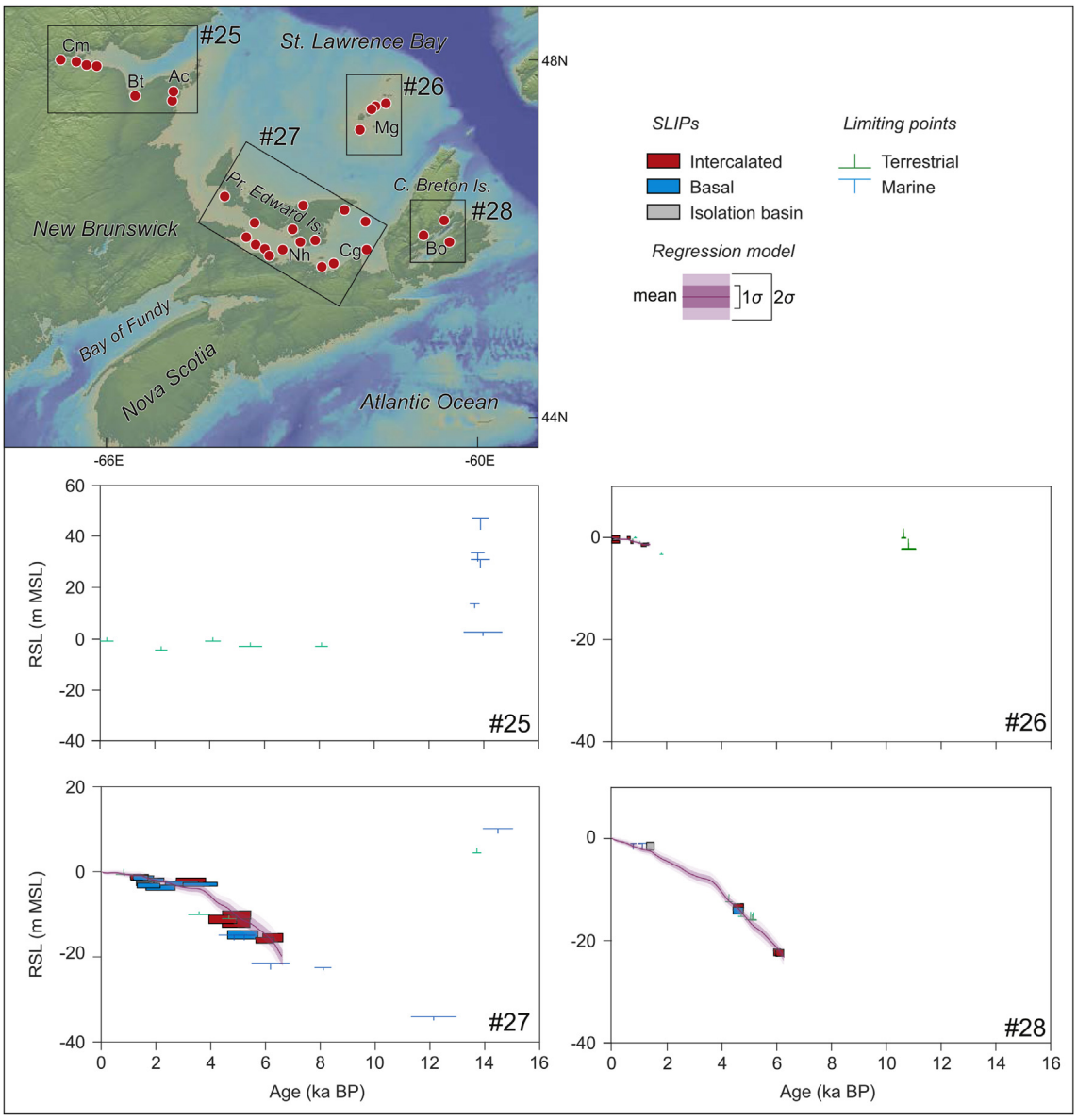

Fig. 9. RSL reconstructions and spatio-temporal statistical model predictions in the northern portion of New Brunswick and Nova Scotia (regions 25 to 28), plotted as in Fig. 4. Cm is western Chaleur Bay, Bt is Bathurst, Ac is Acadia peninsula, Mg are Magdalen islands, Nh is Northumberland Strait, Cg is Cape George, Bo is Lake Bras d'Or.

5.3. Subsiding regions

A different postglacial RSL evolution characterizes regions located at the margin of the former LIS in western Nova Scotia (Fig. 9, region and Fig. 10, regions 30 to 32). Here, our database (SLIPs n = 42; limiting points n = 42) documents well the RSL evolution, at least in the Holocene period. SLIPs were produced using intertidal sediments (salt-marsh peats) and isolation basins. In these regions, no evidence of RSL above present is reported and a continuous RSL rise is recorded for the whole postglacial period. This is due to the combined effects of rising global mean sea level and the progressive collapse of the peripheral forebulge (e.g., Liverman, 1994; Gehrels et al., 2004; Daly et al., 2007), which triggered increasing GIA-related subsidence rates as a function of the distance from the former ice-sheet on both coasts of North America (Barnhardt et al., 1995; Engelhart and Horton, 2012; Engelhart et al., 2015).

Our new compilation has produced well-constrained RSL reconstructions for the last ~9 ka for the outer part of Nova Scotia (regions 28, 30, 31 and 32, Figs. 9 and 10), where the maximum GIA-related subsidence for the entire eastern Canadian dataset is expected (Roy and Peltier, 2015). The most complete record is found in eastern Nova Scotia (region 30) where a suite of mid-Holocene SLIPs documents the progressive RSL rise from ~ −34 m at 8.3 ± 0.2 ka, to ~ −21 m at 6.7 ± 0.5 ka and to ~ −9.9 m at 4.2 ± 0.3 ka. RSL continued rising during the late Holocene from ~ −8.1 m at 3.8 ± 0.5 ka to ~ −3.3 m at 1.7 ± 0.3 ka and finally to the present. The RSL record from the Sable Island region (region 31, Fig. 10) is particularly interesting and unique because this crescent-shaped sandbar outcrops at the extreme limit of the Scotian Shelf (Scott et al., 1984; Fig. 10). Here, RSL was at ~ −35 m at ~9.0 ± 0.5 ka as indicated by both SLIPs and limiting points. RSL continues rising through the Holocene with RSL at ~ −13.3 and at ~ −10.9 m at 5.2 ± 0.6 and at 4.4 ± 0.4 ka, respectively. This RSL history, within uncertainty, is comparable to the one in eastern Nova Scotia (region 30, Fig. 10), implying minimal changes in the isostatic pattern of a

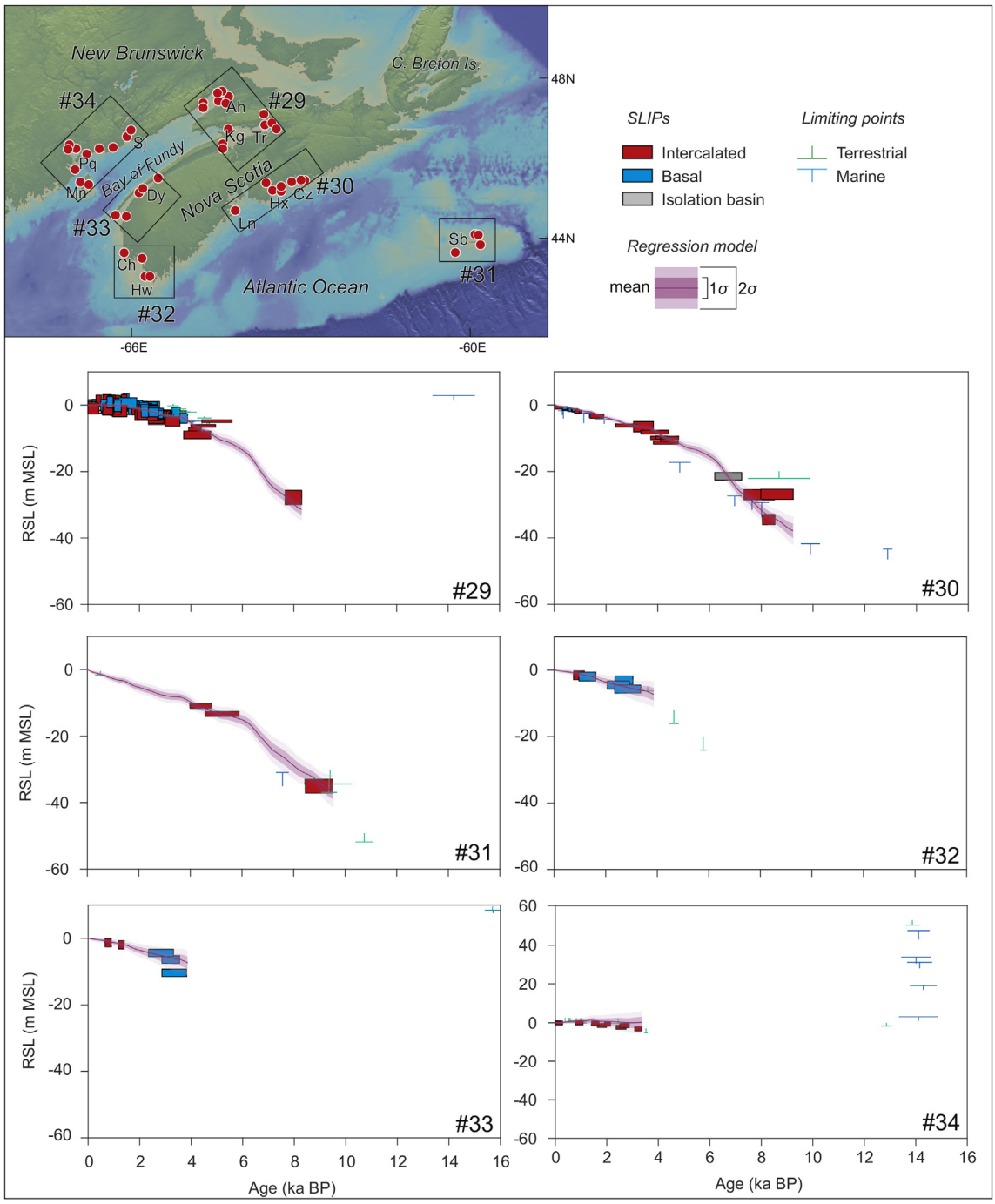

Fig. 10. RSL reconstructions and spatio-temporal statistical model predictions in the southern portion of New Brunswick and Nova Scotia (regions 29 to 34), plotted as in Fig. 4. Ah is Amherst Point, Tr is Truro, Kg is Kingsport. Cz is Chezzetcook Inlet, Hx is Halifax, Ln is Lunenburg, Sb is Sable Island, Hw is Hawk Point, Ch is Chebogue Harbour, Dy is Digby, Sj is St. John, Pm is Passamaquoddy Bay and Mn are Ministers Islands.

large sector of the Scotian Shelf.

6. Holocene rates of relative sea-level change

The combination of a database of SLIPs with good spatial and temporal coverage with a spatio-temporal model allows us to calculate the variability in rates of RSL through time for our records. This analysis is restricted to the Holocene, as there are not enough SLIPs in the late Pleistocene timeframe (see section 5, Fig. 2). Holocene rates are calculated as average rates of change at 1 ka time-steps (Fig. 11). The model can produce estimates of change regardless of data availability, but the rates are particularly robust where suites of SLIPs are available and well distributed throughout the Holocene (such as in region 22 or region 30). At sites where we have a very limited number of SLIPs (i.e., the Labrador coast), we are not able to robustly define the rates of change. Furthermore, early-Holocene SLIPs are restricted to the St. Lawrence corridor, western Newfoundland and outer Nova Scotia. Conversely, the spatial

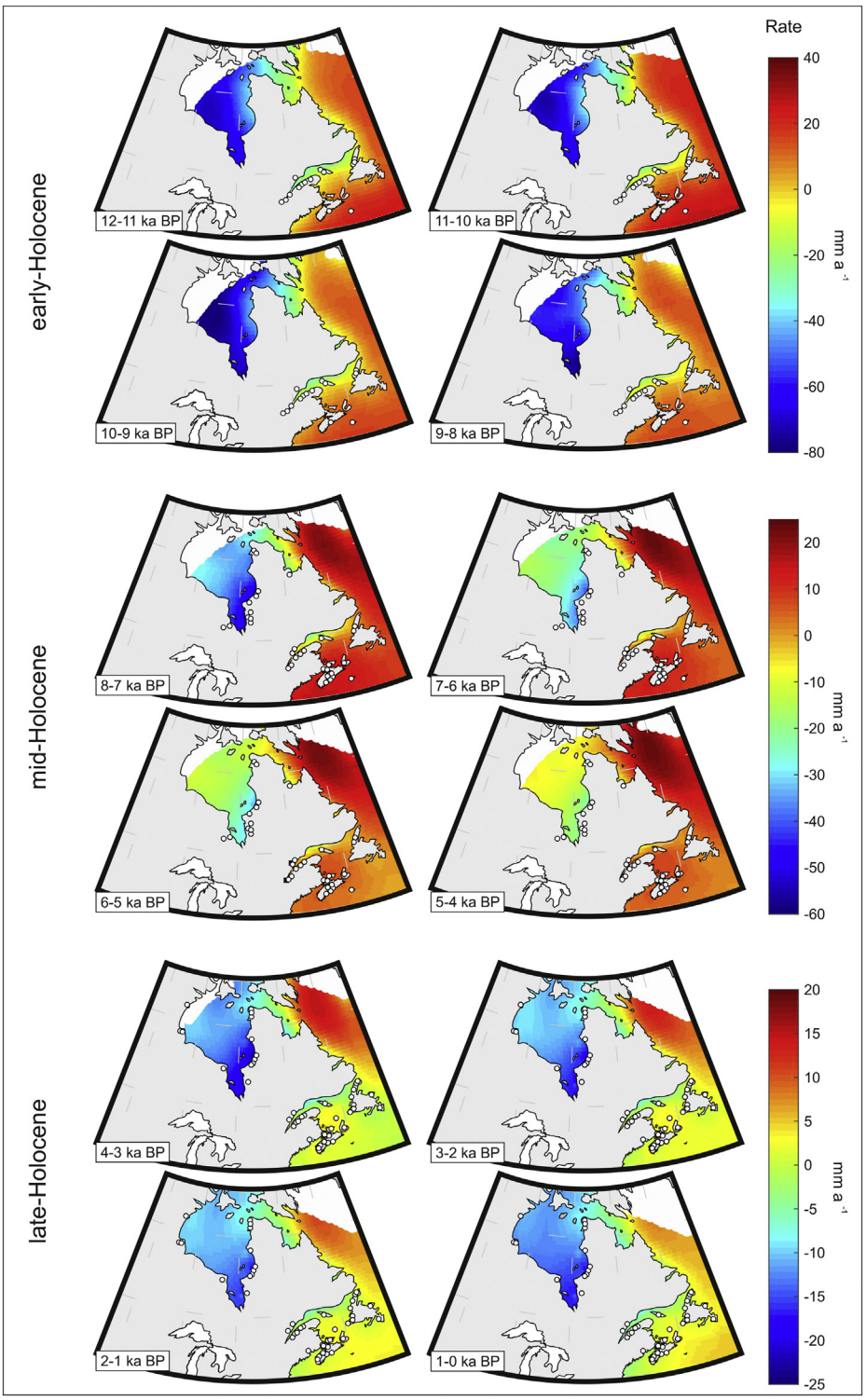

Fig. 11. Mean estimates of rates of RSL change calculated from the spatio-temporal statistical model in early (12–8 ka BP), mid (8–4 ka BP) and late Holocene (4–0 ka BP) along the eastern Canadian coast. White dots indicate the approximate position of the SLIPs. Note changes in scale between early, mid, and late Holocene.

distribution of mid-to late-Holocene SLIPs covers the entire spatial area of the analysis (Fig. 11). For this reason, higher confidence can be placed in the reconstructed rates of RSL rise during the last 8 ka.

The comprehensive analysis of the RSL change rates along the NE Canadian coast show a very coherent spatial pattern in both the mid (8–4 ka BP) and late (4 ka BP to AD 1900) Holocene (Fig. 12). Regional differences in maximum ice-sheet thickness (e.g., Dyke, 2004; Simon et al., 2016), timing of deglaciation (e.g., Tarasov and Peltier, 2004; Dyke et al., 2005; Shaw et al., 2006) and collapse rate of the proglacial forebulge (e.g., Gehrels et al., 2004; Daly et al., 2007) largely control the pattern of changing rates of RSL at millennial timescales. GIA drives land uplift (negative rates) in areas under the former LIS and land subsidence (positive rates) in peripheral areas as the forebulge, beyond the former ice-sheet

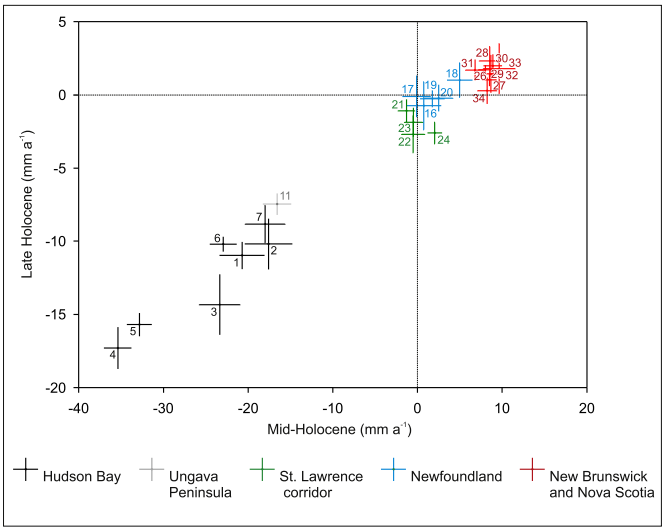

Fig. 12. Comparison of the rate of relative sea-level (RSL) rise over mid (8–4 ka BP) and late (4–0 ka BP) Holocene time periods within the database. Numbers refer to regions discussed within the text. The dashed lines indicate zero vertical movements.

margin, collapses (e.g., Roy and Peltier, 2017).

Our analyses reveal that the highest rate of RSL fall occurred in Hudson Bay and on the Ungava Peninsula, exceeding 30 mm a^{-1} during the mid to late-Holocene. Over the last 8 ka, we can identify spatial variability within these coastal sectors with the highest rate of RSL fall (35 ± 1.6 mm a^{-1}) occurring in the southeastern Hudson Bay and reduced rates ($\leq 23 \pm 1.6$ mm a^{-1}) in the other sections of the bay and over much of the Ungava Peninsula (Fig. 11). The spatial pattern remains the same in the late Holocene (last 4 ka), while rates continue to decline, due to the exponential form of the GIA response, with rates of 15 ± 1.6 mm a^{-1} in the southeastern sector and of 11 ± 0.9 to 9 ± 1.3 mm a^{-1} in the other sections of the bay (Fig. 11). Fig. 12 demonstrates that the variability of GIA-driven falling rates of RSL observed at Hudson Bay and Ungava peninsula are entirely controlled by the distance of each region from the centre of the former ice sheet (regions 4 and 5).

The Newfoundland and St Lawrence corridor regions represent a hinge line of GIA-related vertical motions not only in the modern records (e.g., Sella et al., 2007; Argus et al., 1999; Argus and Peltier, 2010; Peltier et al., 2015; Roy and Peltier, 2017) but demonstrated by the data to have been true since the mid to late-Holocene (Fig. 12). The good temporal and spatial coverage of SLIPs in Newfoundland allowed the rigorous assessment of late-Holocene variability in rates of RSL change. There is a distinct spatial pattern across Newfoundland over this time with rates of RSL rise up to 1.0 ± 1.2 mm a^{-1} in the southern and eastern areas and a RSL fall of up to 0.7 ± 1.6 mm a^{-1} along the northwestern coast (Fig. 11). This further confirms the transitional nature of the Newfoundland coast from a GIA perspective (Liverman, 1994; Shaw and Forbes, 1995; Shaw and Potter, 2015) with rates of land submergence increasing in the southeastern sector due to the collapse of the peripheral forebulge (Shaw et al., 1998; Billy et al., 2015; Love et al., 2016).

In the St Lawrence corridor, RSL dropped very rapidly in early-Holocene with rates up to 22 ± 1.5 mm a^{-1} recorded in the inner St Lawrence region (24, Fig. 11). The fall in RSL slowed significantly between ~10 and 9 ka reaching approximate RSL stability around ~8 ka. This time period is followed by a switch to rising rates of RSL at 2.0 ± 0.9 mm a^{-1} until a RSL highstand was achieved at ~6 to ~4 ka before falling slowly to present at an average rate that did not exceed 2.7 ± 1.2 mm a^{-1}.

Most of the remaining regions from New Brunswick and Nova Scotia have excellent temporal coverage of SLIPs, notably in the mid-to late-Holocene period. These records are marked by a rise of RSL during the early-Holocene, with the highest rates in the easternmost regions (up to 17 ± 2 mm a^{-1}, Fig. 11). RSL slowed down significantly in the mid-Holocene to average rates not exceeding 8.9 ± 1.1 mm a^{-1}. RSL slowed further during the late Holocene, with average rates $<2.0 \pm 0.8$ mm a^{-1}, and the lowest rates in the northern and western Bay of Fundy regions (29 and 34) between ~0.3 ± 0.9 to 1.0 ± 0.5 mm a^{-1} (Fig. 11). Our data indicate that the continuous rising trend observed in these regions slowed significantly in the mid-Holocene (Fig. 11). This reduction in the rate of rise is predominantly driven by the decrease in sea-level equivalent land-ice inputs in the mid-Holocene, coincident with final melting of the Laurentide Ice-sheet at ~7 ka (e.g., Peltier, 1998; Carlson et al., 2008; Renssen et al., 2009), consistent with results from further south along the US Atlantic coast (e.g., Engelhart and Horton, 2012). A further late-Holocene decrease in the rate of RSL rise is observed in these regions (Fig. 11). The variability in the rates (Fig. 12), highest in the eastern coast of Nova Scotia, mainly reflects the influence of the collapsing forebulge in this sector of Atlantic Canada (e.g., Gehrels et al., 2004), which became the dominant process in the last 4 ka (Peltier, 2004; Milne et al., 2005; Engelhart et al., 2009).

7. Conclusions

We have carried out a comprehensive and critical analysis of the postglacial RSL data from eastern Canada, ranging from the Hudson Bay to the border with the USA. This has allowed us to compare and contrast data from different geomorphological contexts in order to obtain basin-scale insights into the processes driving postglacial RSL changes. Our database spans the last ~16.0 ka, with the number SLIPs and limiting points significantly increasing in the last ~12.0 ka. We added new data for 34 regions to previous compilations by reinterpreting and standardizing the various types of RSL indicators to provide an improved framework to produce RSL data at high latitudes using a wide range of proxies. We further correct for effects of local processes (e.g., tidal range change, storm offset) and use a spatio-temporal statistical model to assess patterns and rates of RSL change through time. Our data better constrain the role of the spatially-variable GIA that dominated the postglacial RSL evolution in eastern Canada. In this sector of North America, we observed continuous RSL fall in Hudson Bay and at latitude $\geq$ ~50° N. At lower latitudes, the data defines two non-monotonic RSL patterns. In St. Lawrence corridor regions, RSL dropped to near present levels in the early-Holocene, followed by a mid-Holocene highstand, and then a gradual drop to the present. Around New Brunswick, Bay of Fundy, and along much of the Newfoundland coast, RSL dropped to a spatially variable late-Pleistocene/early-Holocene lowstand followed by a continuous RSL rise in the remaining part of the Holocene period. At the margin of the former ice-sheet extension (eastern Nova Scotia) our data delineate a continuous postglacial RSL rise. We also identified regions, like the Labrador coast and part of St Lawrence corridor, where further investigation is required to better constrain RSL evolution. Such investigations, carried out using the proposed framework employed herein will produce homogeneous and comparable RSL data, thereby enabling a more meaningful assessment of RSL variability along the eastern Canadian coast.

Acknowledgements

The compilation of the database was motivated by discussions at the workshops of PALSEA 2 (PAGES/INQUA/WUN working group),

IGCP Project 639, Holsea (INQUA-CMP1601), Late Quaternary Records Of Coastal Inundation Due To Earth Surface Deformation, Tsunami, And Storms (INQUA CMP 1701P) and MOPP-Medflood (INQUA CMP 1603P). ELA and REK were supported by NSF grants OCE-1458904 and OCE-1702587. The research of WRP at the University of Toronto is supported by NSERC Discovery Grant A9627. BPH and KR were supported by Singapore Ministry of Education Academic Research Fund Tier 1 RG119/17, National Research Foundation Singapore and the Singapore Ministry of Education under the Research Centres of Excellence initiative. This work is Earth Observatory of Singapore contribution no. 214. Finally, we thank the three anonymous reviewer whose comments greatly improved the final version of the paper.

Appendix A. Supplementary data

Supplementary data to this article can be found online at https://doi.org/10.1016/j.quascirev.2018.09.043.

References

Allard, M., Tremblay, G., 1983. Les processus d'érosion littorale périglaciaire de la région de Poste-de-la-Baleine et des îles Manitounuk sur la côte est de la mer d'Hudson, Canada. Zeitschrift für Geomorphologie. Supplement 47, 27–60.
Anthony, E.J., 2008. Shore Processes and Their Palaeoenvironmental Applications, vol. 4. Elsevier.
Andrews, J.T., 1973. Maps of the maximum postglacial marine limit and rebound for the former Laurentide Ice Sheet (The National Atlas of Canada). Arct. Alp. Res. 41–48.
Andrews, J.T., Falconer, G., 1969. Late glacial and post-glacial history and emergence of the Ottawa islands, Hudson bay, northwest territories: evidence on the deglaciation of Hudson bay. Can. J. Earth Sci. 6 (5), 1263–1276.
Arbic, B.K., St-Laurent, P., Sutherland, G., Garrett, C., 2007. On the resonance and influence of the tides in Ungava bay and Hudson strait. Geophys. Res. Lett. 34 (17).
Argus, D.F., Peltier, W.R., 2010. Constraining models of postglacial rebound using space geodesy: a detailed assessment of model ICE-5G (VM2) and its relatives. Geophys. J. Int. 181 (2), 697–723.
Argus, D.F., Peltier, W.R., Watkins, M.M., 1999. Glacial isostatic adjustment observed using very long baseline interferometry and satellite laser ranging geodesy. J. Geophys. Res.: Solid Earth 104 (B12), 29077–29093.
Barber, D.C., Dyke, A., Hillaire-Marcel, C., Jennings, A.E., Andrews, J.T., Kerwin, M.W., Bilodeau, G., McNeely, R., Southon, J., Morehead, M.D., Gagnon, J.M., 1999. Forcing of the cold event of 8,200 years ago by catastrophic drainage of Laurentide lakes. Nature 400 (6742), 344.
Barnett, R.L., Garneau, M., Bernatchez, P., 2016. Salt-marsh sea-level indicators and transfer function development for the Magdalen Islands in the Gulf of St. Lawrence, Canada. Mar. Micropaleontol. 122, 13–26.
Barnett, R.L., Bernatchez, P., Garneau, M., Juneau, M.N., 2017. Reconstructing late Holocene relative sea-level changes at the Magdalen Islands (Gulf of St. Lawrence, Canada) using multi-proxy analyses. J. Quat. Sci. 32 (3), 380–395.
Barnhardt, W.A., Gehrels, W.R., Kelley, J.T., 1995. Late Quaternary relative sea-level change in the western Gulf of Maine: evidence for a migrating glacial forebulge. Geology 23 (4), 317–320.
Batterson, M.J., Taylor, D.M., 2003. Regional till geochemistry and surficial geology of the western Avalon peninsula and isthmus. Newfoundland department of mines and energy, St. John's. Geol. Surv. Rep. 03– 1, 259–272.
Bell, T., Batterson, M.J., Liverman, D.G., Shaw, J., 2003. A new late-glacial sea-level record for St. George's Bay, Newfoundland. Can. J. Earth Sci. 40 (8), 1053–1070.
Bell, T., Smith, I.R., Renouf, M.A.P., 2005. Postglacial sea-level history and coastline change at Port au Choix, Great Northern Peninsula, Newfoundland. Nfld. Labrador Stud. 20 (1).
Billy, J., Robin, N., Hein, C.J., Certain, R., Fitzgerald, D.M., 2015. Insight into the late Holocene sea-level changes in the NW Atlantic from a paraglacial beach-ridge plain south of Newfoundland. Geomorphology 248, 134–146.
Bradley, S.L., Milne, G.A., Horton, B.P., Zong, Y., 2016. Modelling sea level data from China and Malay-Thailand to estimate Holocene ice-volume equivalent sea level change. Quat. Sci. Rev. 137, 54–68.
Brooks, A., Edwards, R., 2006. The development of a sea-level database for Ireland. Ir. J. Earth Sci. 13–27.
Brown MacPherson, J., 1996. Delayed deglaciation by downwasting of the Northeast Avalon Peninsula, Newfoundland: an application of the early postglacial pollen record. Géogr. Phys. Quaternaire 50 (2), 201–220.
Carlson, A.E., Clark, P.U., Raisbeck, G.M., Brook, E.J., 2007. Rapid Holocene deglaciation of the labrador sector of the Laurentide ice-sheet. J. Clim. 20 (20), 5126–5133.
Carlson, A.E., LeGrande, A.N., Oppo, D.W., Came, R.E., Schmidt, G.A., Anslow, F.S., et al., 2008. Rapid early Holocene deglaciation of the Laurentide ice-sheet. Nat. Geosci. 1 (9), 620.
Catto, N.R., Griffiths, H., Jones, S., Porter, H., 2000. Late Holocene Sea Level changes, eastern Newfoundland. Current research, Newfoundland department of mines and energy. Geol. Surv. Rep. 1, 49–59.
Catto, N.R., Taylor, D.M., 1998. Landforms and surficial geology of the Argentia map sheet (NTS 1N/05), Newfoundland. Scale 1 (50).
Cauchon-Voyer, G., Locat, J., St-Onge, G., 2008. Late-quaternary morpho-sedimentology and submarine mass movements of the betsiamites area, lower St. Lawrence estuary, Quebec, Canada. Mar. Geol. 251 (3), 233–252.
Clark, P.U., Fitzhugh, W., 1990. Late deglaciation of the central Labrador coast and its implications for the age of glacial lakes Naskaupi and McLean and for prehistory. QR (Quat. Res.) (N. Y.) 34 (3), 296–305.
Clark, J.A., Farrell, W.E., Peltier, W.R., 1978. Global changes in postglacial sea level: a numerical calculation 1. QR (Quat. Res.) (N. Y.) 9 (3), 265–287.
Clarke, G.K., Leverington, D.W., Teller, J.T., Dyke, A.S., 2004. Paleohydraulics of the last outburst flood from glacial Lake Agassiz and the 8200 BP cold event. Quat. Sci. Rev. 23 (3–4), 389–407.
Coulthard, R.D., Furze, M.F., Pieńkowski, A.J., Nixon, F.C., England, J.H., 2010. New marine ΔR values for Arctic Canada. Quat. Geochronol. 5 (4), 419–434.
Cronin, T.M., 1979. Late Pleistocene benthic foraminifers from the St. Lawrence lowlands. J. Paleontol. 781–814.
Daigneault, R.A., 2008. Géologie du Quaternaire du nord de la péninsule d'Ungava, Québec; Commission géologique du Canada. Bulletin 533, 115 pp.
Daly, J.F., Belknap, D.F., Kelley, J.T., Bell, T., 2007. Late Holocene sea-level change around Newfoundland. Can. J. Earth Sci. 44 (10), 1453–1465.
Dionne, J.C., 1977. La mer de Goldthwait au Québec. Géogr. Phys. Quaternaire 31 (1–2), 61–80.
Dionne, J.C., 1988. Holocene relative sea-level fluctuations in the St. Lawrence estuary, Québec, Canada. QR (Quat. Res.) (N. Y.) 29 (3), 233–244.
Dionne, J.C., 1990. Observations sur le niveau marin relatif à l'Holocène, à Rivière-du-Loup, estuaire du Saint-Laurent, Québec. Géogr. Phys. Quaternaire 44 (1), 43–53.
Dionne, J.-C., 1996. La terrasse Mitis à la pointe aux Alouettes, côte nord du moyen estuaire du Saint-Laurent. Géogr. Phys. Quaternaire 50, 57–72.
Dionne, J.C., 1997. Nouvelles données sur la transgression Laurentienne, côte sud du moyen estuaire du Saint-Laurent, Québec. Géogr. Phys. Quaternaire 51 (2), 201–210.
Dionne, J.C., 1999. Indices de fluctuations mineures du niveau marin relatif à l'Holocène supérieur, à L'Isle-Verte, côte sud de l'estuaire du Saint-Laurent, Québec. Géogr. Phys. Quaternaire 53 (2), 277–285.
Dionne, J.C., Coll, D., 1995. Le niveau marin relatif dans la région de Matane (Québec), de la déglaciation à nos jours. Géogr. Phys. Quaternaire 49 (3), 363–380.
Dionne, J.C., Dubois, J.M., Bernatchez, P., 2004. La terrasse Mitis à la pointe de Mille-Vaches (Péninsule de Portneuf), rive nord de l'estuaire maritime du Saint-Laurent: nature des dépôts et évolution du niveau marin relatif à l'Holocène. Géogr. Phys. Quaternaire 58 (2–3), 281–295.
Dionne, J.C., 2001. Troncs d'arbres fossiles sur la batture de l'anse de Bellechasse (Québec): indice d'une fluctuation mineure du niveau marin relatif à l'Holocène supérieur. Géogr. Phys. Quaternaire 55 (3), 301–306.
Dutton, A., Carlson, A.E., Long, A.J., Milne, G.A., Clark, P.U., DeConto, R., Horton, B.P., Rahmstorf, S., Raymo, M.E., 2015. Sea-level rise due to polar ice-sheet mass loss during past warm periods. Science 349 (6244), aaa4019.
Dyke, A.S., 2004. An outline of North American deglaciation with emphasis on central and northern Canada. Dev. Quat. Sci. 2, 373–424.
Dyke, A.S., Andrews, J.T.A., Clark, P.U., England, J.H., Miller, G.H., Shaw, J., Veillette, J.J., 2002. The Laurentide and innuitian ice sheets during the last glacial maximum. Quat. Sci. Rev. 21, 9–31.
Dyke, A., Dredge, L., Hodgson, D., 2005. North American deglacial marine-and lake-limit surfaces. Géogr. Phys. Quaternaire 59 (2–3), 155–185.
Dyke, A.S., Peltier, W.R., 2000. Forms, response times and variability of relative sea-level curves, glaciated North America. Geomorphology 32 (3–4), 315–333.
Dyke, A., Prest, V., 1987. Late wisconsinan and Holocene history of the Laurentide ice-sheet. Géogr. Phys. Quaternaire 41 (2), 237–263.
Edwards, R., Gehrels, W.R., Brooks, A., Fyfe, R., Pullen, K., Kuchar, J., Craven, K., 2017. Resolving discrepancies between field and modelled relative sea-level data: lessons from western Ireland. J. Quat. Sci. 32 (7), 957–975.
Egbert, G.D., Erofeeva, S.Y., 2002. Efficient inverse modeling of barotropic ocean tides. J. Atmos. Ocean. Technol. 19 (2), 183–204.
Engelhart, S.E., Horton, B.P., 2012. Holocene sea level database for the Atlantic coast of the United States. Quat. Sci. Rev. 54, 12–25.
Engelhart, S.E., Horton, B.P., Douglas, B.C., Peltier, W.R., Törnqvist, T.E., 2009. Spatial variability of late Holocene and 20th century sea-level rise along the Atlantic coast of the United States. Geology 37 (12), 1115–1118.
Engelhart, S.E., Vacchi, M., Horton, B.P., Nelson, A.R., Kopp, R.E., 2015. A sea-level database for the Pacific coast of central North America. Quat. Sci. Rev. 113, 78–92.
England, J., Atkinson, N., Bednarski, J., Dyke, A.S., Hodgson, D.A., Ó Cofaigh, C., 2006. The Innuitian Ice Sheet: configuration, dynamics and chronology. Quat. Sci. Rev. 25, 689–703.
England, J., Dyke, A.S., Coulthard, R.D., Mcneely, R., Aitken, A., 2013. The exaggerated radiocarbon age of deposit-feeding molluscs in calcareous environments. Boreas 42 (2), 362–373.
Fereidoni, A., Atkinson, G.M., 2015. Correlation between coulomb stress changes imparted by historic earthquakes and current seismicity in Charlevoix seismic

zone, eastern Canada. Seismol Res. Lett. 86 (1), 272–284.
Fillon, R.H., 1975. Deglaciation of the Labrador continental shelf. Nature 253 (5491), 429–431.
Fitzhugh, W., 1977. Population movement and culture change on the central Labrador coast. Ann. N. Y. Acad. Sci. 288 (1), 481–497.
Fleming, K., Johnston, P., Zwartz, D., Yokoyama, Y., Lambeck, K., Chappell, J., 1998. Refining the eustatic sea-level curve since the Last Glacial Maximum using far- and intermediate-field sites. Earth Planet Sci. Lett. 163 (1), 327–342.
Forbes, D.L., 1984. Coastal geomorphology and sediments of Newfoundland. Current research, part B. Geol. Surv. Can. Pap. 11–24.
Fraser, C., Hill, P.R., Allard, M., 2005. Morphology and facies architecture of a falling sea level strandplain, Umiujaq, Hudson Bay, Canada. Sedimentology 52 (1), 141–160.
Gehrels, W.R., 2000. Using foraminiferal transfer functions to produce high-resolution sea-level records from salt-marsh deposits, Maine, USA. Holocene 10 (3), 367–376.
Gehrels, W.R., Long, A.J., 2007. Quaternary land–ocean interactions: sea-level change, sediments and tsunami. Mar. Geol. 242 (1), 1–4.
Gehrels, W.R., Belknap, D.F., Pearce, B.R., Gong, B., 1995. Modeling the contribution of M2 tidal amplification to the Holocene rise of mean high water in the Gulf of Maine and the Bay of Fundy. Mar. Geol. 124 (1–4), 71–85.
Gehrels, W.R., Milne, G.A., Kirby, J.R., Patterson, R.T., Belknap, D.F., 2004. Late Holocene sea-level changes and isostatic crustal movements in Atlantic Canada. Quat. Int. 120 (1), 79–89.
Gehrels, W.R., Kirby, J.R., Prokoph, A., Newnham, R.M., Achterberg, E.P., Evans, H., Black, S., Scott, D.B., 2005. Onset of recent rapid sea-level rise in the western Atlantic Ocean. Quat. Sci. Rev. 24 (18-19), 2083–2100.
Glaser, P.H., Hansen, B., Siegel, D.I., Reeve, A.S., Morin, P.J., 2004. Rates, pathways and drivers for peatland development in the Hudson Bay Lowlands, northern Ontario, Canada. J. Ecol. 92 (6), 1036–1053.
Goslin, J., Lanoë, B.V.V., Spada, G., Bradley, S., Tarasov, L., Neill, S., Suanez, S., 2015. A new Holocene relative sea-level curve for western Brittany (France): insights on isostatic dynamics along the Atlantic coasts of north-western Europe. Quat. Sci. Rev. 129, 341–365.
Gosling, E., 1992. Systematics and geographic distribution of *Mytilus*. The Mussel Mytilus; Ecology, physiology, genetic and culture. Dev. Aquacult. Fish. Sci. 25.
Gray, J.T., Lauriol, B., 1985. Dynamics of the late Wisconsin ice-sheet in the Ungava Peninsula interpreted from geomorphological evidence. Arct. Alp. Res. 289–310.
Gray, J., de Boutray, B., Hillaire-Marcel, C., Lauriol, B., 1980. Postglacial emergence of the west coast of Ungava bay, Quebec. Arct. Alp. Res. 19–30.
Gray, J., Lauriol, B., Bruneau, D., Ricard, J., 1993. Postglacial emergence of Ungava Peninsula, and its relationship to glacial history. Can. J. Earth Sci. 30 (8), 1676–1696.
Grant, D.R., 1980. Quaternary sea-level change in Atlantic Canada as an indication of crustal delevelling. In: Morner, N.A. (Ed.), Earth Rheology, Isostasy and Eustasy, pp. 201–214.
Grant, D.R., 1989. Quaternary geology of the atlantic appalachian region of Canada. In: Fulton, R.J. (Ed.), Quaternary Geology of Canada and Greenland. Geological Survey of Canada, pp. 393–440 no. 1.
Grant, D.R., 1994. Quaternary Geology of Port Saunders Map Area, Newfoundland. Geological Survey of Canada, Ottawa. Paper 91-20, 59 pp.
Griffiths, S.D., Peltier, W.R., 2009. Modeling of polar ocean tides at the Last Glacial Maximum: amplification, sensitivity, and climatological implications. J. Clim. 22 (11), 2905–2924.
Han, H.K., Gomez, N., 2018. The impact of water loading on postglacial decay times in Hudson Bay. Earth Planet Sci. Lett. 489, 156–165.
Hardy, L., 1976. Contribution a l'etude geomorphologique de la portion Quebecoise de la Baie de James. PhD thesis. McGill University, Montreal.
Hijma, M., Engelhart, S.E., Törnqvist, T.E., Horton, B.P., Hu, P., Hill, D.F., 2015. In: Shennan, I., Long, A.J., Horton (Eds.), A Protocol for a Geological Sea-level Database. Handbook of Sea-level Research. BP, Wiley Blackwell, pp. 536–553.
Hill, D.F., 2016. Spatial and temporal variability in tidal range: evidence, causes, and effects. Current Clim. Change Rep. 2 (4), 232–241.
Hill, D.F., Griffiths, S.D., Peltier, W.R., Horton, B.P., Törnqvist, T.E., 2011. High-resolution numerical modeling of tides in the western atlantic, Gulf of Mexico, and caribbean sea during the Holocene. J. Geophys. Res.: Oceans 116 (C10).
Hill, P.R., Meulé, S., Longuépée, H., 2003. Combined-flow processes and sedimentary structures on the shoreface of the wave-dominated Grande-rivière-de-la-baleine delta. J. Sediment. Res. 73, 217–226.
Hillaire-Marcel, C., 1976. La déglaciation et le relèvement isostatique sur la côte est de la baie d'Hudson. Cah. Geograph. Quebec 20 (50), 185–220.
Hillaire-Marcel, C., Fairbridge, R.W., 1978. Isostasy and eustasy of Hudson bay. Geology 6 (2), 117–122.
Hillaire-Marcel, C., Occhietti, S., 1977. Fréquence des datations au 14C de faunes marines post-glaciaires de l'Est du Canada et variations paléoclimatiques. Palaeogeogr. Palaeoclimatol. Palaeoecol. 21 (1), 17–54.
Horton, B.P., Shennan, I., 2009. Compaction of Holocene strata and the implications for relative sealevel change on the east coast of England. Geology 37 (12), 1083–1086.
Horton, B.P., Peltier, W.R., Culver, S.J., Drummond, R., Engelhart, S.E., Kemp, A.C., et al., 2009. Holocene sea-level changes along the North Carolina Coastline and their implications for glacial isostatic adjustment models. Quat. Sci. Rev. 28 (17), 1725–1736.
Horton, B.P., Engelhart, S.E., Kemp, A.C., Sawai, Y., 2013. Microfossils in tidal settings as indicators of sea-level change, paleoearthquakes, tsunamis, and tropical cyclones. In: Shroder, John F. (Ed.), Treatise on Geomorphology, vol. 14. Academic Press, San Diego, pp. 292–314.
Karegar, M.A., Dixon, T.H., Engelhart, S.E., 2016. Subsidence along the atlantic coast of North America: insights from GPS and late Holocene Relative Sea level data. Geophys. Res. Lett. 43 (7), 3126–3133.
Kemp, A.C., Telford, R.J., 2015. Transfer functions. In: Shennan, I., Long, A., Horton, B.P. (Eds.), Handbook of Sea Level Research. Wiley, pp. 470–499.
Kemp, A.C., Wright, A.J., Barnett, R.L., Hawkes, A.D., Charman, D.J., Sameshima, C., van de Plassche, O., 2017. Utility of salt-marsh foraminifera, testate amoebae and bulk-sediment δ 13 C values as sea-level indicators in Newfoundland, Canada. Mar. Micropaleontol. 130, 43–59.
Khan, N.S., Ashe, E., Horton, B.P., Dutton, A., Kopp, R.E., Brocard, G., Engelhart, S.E., Hill, D.F., Peltier, W.R., Vane, C.H., Scatena, F.N., 2017. Drivers of Holocene Sea-level change in the caribbean. Quat. Sci. Rev. 155, 13–36.
Khan, N.S., Ashe, E., Shaw, T.A., Vacchi, M., Walker, J., Peltier, W.R., Kopp, R.E., Horton, B.P., 2015. Holocene relative sea-level changes from near-, intermediate-, and far-field locations. Current Climate Change Reports 1 (4), 247–262.
Kopp, R.E., Kemp, A.C., Bittermann, K., Horton, B.P., Donnelly, J.P., Gehrels, W.R., et al., 2016. Temperature-driven global sea-level variability in the Common Era. Proc. Natl. Acad. Sci. Unit. States Am. 113 (11), E1434–E1441.
Kopp, R.E., Simons, F.J., Mitrovica, J.X., Maloof, A.C., Oppenheimer, M., 2009. Probabilistic assessment of sea level during the last interglacial stage. Nature 462, 863–867.
Kranck, K., 1972. Geomorphological development and post-Pleistocene sea level changes, Northumberland Strait, Maritime Provinces. Can. J. Earth Sci. 9, 835–844.
Lambeck, K., Rouby, H., Purcell, A., Sun, Y., Sambridge, M., 2014. sea Level and global ice volumes from the last glacial maximum to the Holocene. Proc. Natl. Acad. Sci. Unit. States Am. 111 (43), 15296–15303.
Lajeunesse, P., Allard, M., 2003. Late quaternary deglaciation, glaciomarine sedimentation and glacioisostatic recovery in the Rivière Nastapoka area, eastern Hudson Bay, Northern Québec. Géogr. Phys. Quaternaire 57 (1), 65–83.
Lauriol, B., Gray, J., Hétu, B., Cyr, A., 1979. Le cadre chronologique et paléogéographique de l'évolution marine depuis la déglaciation dans la région d'Aupaluk Nouveau-Québec. Géogr. Phys. Quaternaire 33 (2), 189–203.
Lavoie, C., Allard, M., Duhamel, D., 2012. Deglaciation landforms and C-14 chronology of the Lac Guillaume-Delisle area, eastern Hudson Bay: a report on field evidence. Geomorphology 159, 142–155.
Lemieux, A.M., Bhiry, N., Desrosiers, P.M., 2011. The geoarchaeology and traditional knowledge of winter sod houses in eastern Hudson Bay, Canadian Low Arctic. Geoarchaeology 26 (4), 479–500.
Liverman, D.G., 1994. Relative sea-level history and isostatic rebound in Newfoundland, Canada. Boreas 23 (3), 217–230.
Lloyd, J., 2000. Combined foraminiferal and thecamoebian environmental reconstruction from an isolation basin in NW Scotland: implications for sea level studies. J. Foraminifer. Res. 30, 294e305.
Long, A.J., Woodroffe, S.A., Roberts, D.H., Dawson, S., 2011. Isolation basins, sea-level changes and the Holocene history of the Greenland Ice-sheet. Quat. Sci. Rev. 30 (27), 3748–3768.
Love, R., Milne, G.A., Tarasov, L., Engelhart, S.E., Hijma, M.P., Latychev, K., et al., 2016. The contribution of glacial isostatic adjustment to projections of sea-level change along the Atlantic and Gulf coasts of North America. Earth's Future 4 (10), 440–464.
Luettich Jr., R.A., Westerink, J.J., Scheffner, N.W., 1992. ADCIRC: an Advanced Three-dimensional Circulation Model for Shelves, Coasts, and Estuaries. Report 1. Theory and Methodology of ADCIRC-2DDI and ADCIRC-3DL (No. CERC-TR-DRP-92-6). Coastal Engineering Research Center, Vicksburg MS.
Martindale, A., Morlan, R., Betts, M., Blake, M., Gajewski, K., Chaput, M., Mason, A., Vermeersch, P., 2016. Canadian Archaeological Radiocarbon Database (CARD 2.1). http://www.canadianarchaeology.ca.
Matthews, B., 1966. Radiocarbon dated postglacial land uplift in Northern Ungava, Canada. Nature 211 (5054), 1164–1166.
Matthiessen, G.C., 1960. Intertidal zonation in populations of *Mya arenaria*. Limnol. Oceanogr. 5 (4), 381–388.
McHutchon, A., Rasmussen, C.E., 2011. Gaussian process training with input noise. In: Advances in Neural Information Processing Systems, pp. 1341–1349.
McNeely, R., Brennan, J., 2005. Geological survey of Canada revised shell dates. Geological Survey of Canada. Open File 5019.
McNeely, R., Dyke, A.S., Southon, J.R., 2006. Canadian marine reservoir ages, preliminary data assessment. Geological Survey Canada 3. Open File 5049, 530 pp.
Milne, G.A., Peros, M., 2013. Data–model comparison of Holocene sea-level change in the circum-Caribbean region. Global Planet. Change 107, 119–131.
Milne, G.A., Davis, J.L., Mitrovica, J.X., Scherneck, H.G., Johansson, J.M., Vermeer, M., Koivula, H., 2001. Space-geodetic constraints on glacial isostatic adjustment in Fennoscandia. Science 291 (5512), 2381–2385.
Milne, G.A., Long, A.J., Bassett, S.E., 2005. Modelling Holocene Relative Sea-level observations from the caribbean and South America. Quat. Sci. Rev. 24 (10), 1183–1202.
Milne, G.A., Mitrovica, J.X., Davis, J.L., 1999. Near-field hydro-isostasy: the implementation of a revised sea-level equation. Geophys. J. Int. 139 (2), 464–482.
Milne, G.A., Mitrovica, J.X., Scherneck, H.G., Davis, J.L., Johansson, J.M., Koivula, H., Vermeer, M., 2004. Continuous GPS measurements of postglacial adjustment in Fennoscandia: 2. Modeling results. J. Geophys. Res.: Solid Earth 109 (B2).
Miousse, L., Bhiry, N., Lavoie, M., 2003. Isolation and water-level fluctuations of Lake

kachishayoot, northern Quebec, Canada. QR (Quat. Res.) (N. Y.) 60 (2), 149–161.
Mitrovica, J.X., Milne, G.A., 2002. On the origin of late Holocene sea-level highstands within equatorial ocean basins. Quat. Sci. Rev. 21 (20), 2179–2190.
Mitrovica, J.X., Forte, A.M., Simons, M., 2000. A reappraisal of postglacial decay times from Richmond Gulf and James Bay, Canada. Geophys. J. Int. 142 (3), 783–800.
Occhietti, S., Chartier H, M., Hillaire-Marcel, C., Cournoyer, M., Cumbaa, S., Harington, R., 2001. Paléoenvironnements de la Mer de Champlain dans la région de Québec, entre 11 300 et 9750 BP: le site de Saint-Nicolas. Géogr. Phys. Quaternaire 55 (1), 23–46.
Otvos, E.G., 2000. Beach ridges—definitions and significance. Geomorphology 32 (1), 83–108.
Padgett, J.S., Engelhart, S.E., Hoffmann, G., Rosentau, A., Yu, F., 2018. Sea-level change from minutes to millennia: first meeting of IGCP Project 639 in Oman. Episodes 41 (2), 115–118.
Parent, M., Occhietti, S., 1988. Late wisconsinan deglaciation and Champlain Sea invasion in the St. Lawrence valley, québec. Géogr. Phys. Quaternaire 42 (3), 215–246.
Patterson, R.T., Gehrels, W.R., Belknap, D.F., Dalby, A.P., 2004. The distribution of salt-marsh foraminifera at Little Dipper Harbour New Brunswick, Canada: implications for development of widely applicable transfer functions in sea-level research. Quat. Int. 120 (1), 185–194.
Peltier, W.R., 1998. Postglacial variations in the level of the sea: implications for climate dynamics and solid-earth geophysics. Rev. Geophys. 36 (4), 603–689.
Peltier, W.R., 2002. Global glacial isostatic adjustment: palaeogeodetic and space-geodetic tests of the ICE-4G (VM2) model. J. Quat. Sci. 17 (5-6), 491–510.
Peltier, W.R., 2004. Global glacial isostasy and the surface of the ice-age Earth: the ICE-5G (VM2) model and GRACE. Annu. Rev. Earth Planet Sci. 32, 111–149.
Peltier, W.R., Fairbanks, R.G., 2006. Global glacial ice volume and Last Glacial Maximum duration from an extended Barbados sea level record. Quat. Sci. Rev. 25 (23), 3322–3337.
Peltier, W.R., Argus, D.F., Drummond, R., 2015. Space geodesy constrains ice age terminal deglaciation: the global ICE-6G_C (VM5a) model. J. Geophys. Res.: Solid Earth 120 (1), 450–487.
Pendea, I.F., Costopoulos, A., Nielsen, C., Chmura, G.L., 2010. A new shoreline displacement model for the last 7 ka from eastern James Bay, Canada. QR (Quat. Res.) (N. Y.) 73 (3), 474–484.
Petersen, K.S., 1986. The ertebølle 'køkkenmødding'and the marine development of the limfjord, with particular reference to the Molluscan fauna. Journal of Danish Archaeology 5 (1), 77–84.
Pienitz, R., Lortie, G., Allard, M., 1991. Isolation of lacustrine basins and marine regression in the Kuujjuaq area, northern Québec, as inferred from diatom analysis. Géogr. Phys. Quaternaire 45 (2), 155–174.
Powers, S.P., Bishop, M.A., Grabowski, J.H., Peterson, C.H., 2006. Distribution of the invasive bivalve *Mya arenaria* L. on intertidal flats of southcentral Alaska. J. Sea Res. 55 (3), 207–216.
Preuss, H., 1979. Progress in computer evaluation of sea level data within the IGCP project no. 61. In: Proc. 1978 International Symposium of Coastal Evolution in the Quaternary, pp. 104–134.
Prest, V.K., 1970. Quaternary geology of Canada, chapter 12 of. In: Douglas, R.J.W. (Ed.), Geology and Economic Minerals of Canada. Geological Survey of Canada, Economic Geology Series, No. 1, fifth ed., pp. 675–764.
Rasmussen, C.E., Williams, C.K., 2006. Gaussian Process for Machine Learning. MIT press.
Rampton, V.N., Gauthier, R.C., Thibault, J., Seaman, A.A., 1984. Quaternary geology of new Brunswick. Geological Survey of Canada 416, 1–77. Memoir.
Reimer, P.J., Reimer, R.W., 2001. A marine reservoir correction database and on-line interface. Radiocarbon 43 (2A), 461–463.
Reimer, P.J., Bard, E., Bayliss, A., Beck, J.W., Blackwell, P.G., Ramsey, C.B., et al., 2013. IntCal13 and Marine13 radiocarbon age calibration curves 0–50,000 years cal BP. Radiocarbon 55 (4), 1869–1887.
Rémillard, A.M., St-Onge, G., Bernatchez, P., Hétu, B., Buylaert, J.P., Murray, A.S., Lajeunesse, P., 2017. Relative sea-level changes and glacio-isostatic adjustment on the Magdalen Islands archipelago (Atlantic Canada) from MIS 5 to the late Holocene. Quat. Sci. Rev. 171, 216–233.
Rémillard, A.M., St-Onge, G., Bernatchez, P., Hétu, B., Buylaert, J.P., Murray, A.S., Vigneault, B., 2016. Chronology and stratigraphy of the Magdalen Islands archipelago from the last glaciation to the early Holocene: new insights into the glacial and sea-level history of eastern Canada. Boreas 45 (4), 604–628.
Renssen, H., Seppä, H., Heiri, O., Roche, D.M., Goosse, H., Fichefet, T., 2009. The spatial and temporal complexity of the Holocene thermal maximum. Nat. Geosci. 2 (6), 411.
Rogerson, R.J., Tucker, C.M., 1972. Observations on the Glacial History of the Avalon Peninsula.
Rovere, A., Antonioli, F., Bianchi, C.N., 2015. Fixed Biological Indicators. Handbook of Sea-Level Research, pp. 268–280.
Rovere, A., Raymo, M.E., Vacchi, M., Lorscheid, T., Stocchi, P., Gómez-Pujol, L., et al., 2016. The analysis of last interglacial (MIS 5e) relative sea-level indicators: reconstructing sea-level in a warmer world. Earth Sci. Rev. 159, 404–427.
Roy, K., Peltier, W.R., 2015. Glacial isostatic adjustment, relative sea level history and mantle viscosity: reconciling relative sea level model predictions for the US East coast with geological constraints. Geophys. J. Int. 201 (2), 1156–1181.
Roy, K., Peltier, W.R., 2017. Space-geodetic and water level gauge constraints on continental uplift and tilting over North America: regional convergence of the ICE-6G_C (VM5a/VM6) models. Geophys. J. Int. 210 (2), 1115–1142.
Sander, L., Hede, M.U., Fruergaard, M., Nielsen, L., Clemmensen, L.B., Kroon, A., et al., 2016. Coastal lagoons and beach ridges as complementary sedimentary archives for the reconstruction of Holocene relative sea-level changes. Terra. Nova 28 (1), 43–49.
Scott, D.B., Medioli, F.S., 1982. Micropaleontological documentation for early Holocene fall of relative sea level on the Atlantic coast of Nova Scotia. Geology 10 (5), 278–281.
Scott, D.B., Brown, K., Collins, E.S., Medioli, F.S., 1995. A new sea-level curve from Nova Scotia: evidence for a rapid acceleration of sea-level rise in the late mid-Holocene. Can. J. Earth Sci. 32 (12), 2071–2080.
Scott, D.B., Boyd, R., Medioli, F.S., 1987. Relative Sea-level Changes in Atlantic Canada: Observed Level and Sedimentological Changes Vs. Theoretical Models.
Scott, D.B., Medioli, F.S., Duffett, T.E., 1984. Holocene rise of relative sea level at Sable Island, Nova Scotia, Canada. Geology 12 (3), 173–176.
Scott, D.B., Greenberg, D.A., 1983. Relative sea-level rise and tidal development in the Fundy tidal system. Can. J. Earth Sci. 20 (10), 1554–1564.
Scott, D.B., Williamson, M.A., Duffett, T.E., 1981. Marsh foraminifera of Prince Edward Island: their recent distribution and application for former sea level studies. Marit. Sediments Atl. Geol. 17, 98–129.
Sella, G.F., Stein, S., Dixon, T.H., Craymer, M., James, T.S., Mazzotti, S., Dokka, R.K., 2007. Observation of glacial isostatic adjustment in "stable" North America with GPS. Geophys. Res. Lett. 34 (2).
Shaw, J., Ceman, J., 1999. Salt-marsh aggradation in response to late-Holocene sea-level rise at Amherst Point, Nova Scotia, Canada. Holocene 9 (4), 439–451.
Shaw, J., Forbes, D.L., 1995. The postglacial relative sea-level lowstand in Newfoundland. Can. J. Earth Sci. 32 (9), 1308–1330.
Shaw, J., Amos, C.L., Greenberg, D.A., O'Reilly, C.T., Parrott, D.R., Patton, E., 2010. Catastrophic tidal expansion in the bay of Fundy, Canada earth sciences sector (ESS) contribution 20090423. Can. J. Earth Sci. 47 (8), 1079–1091.
Shaw, J., Potter, D.P., 2015. Surficial geology, coastal waters, island of Newfoundland, Newfoundland and labrador. Geol. Surv. Can. Bull. 605, 118 pp.
Shaw, J., Fader, G.B., Taylor, R.B., 2009. Submerged early Holocene coastal and terrestrial landforms on the inner shelves of Atlantic Canada. Quat. Int. 206 (1-2), 24–34.
Shaw, J., Piper, D.J.W., Fader, G.B.J., King, E.L., Todd, B.J., Bell, T., Batterson, M.J., Liverman, D.G.E., 2006. A conceptual model of the deglaciation of Atlantic Canada. Quat. Sci. Rev. 25 (17), 2059–2081.
Shaw, J., Taylor, R., Forbes, D., 1993. Impact of the Holocene transgression on the atlantic coastline of Nova Scotia. Géogr. Phys. Quaternaire 47 (2), 221–238.
Shaw, J., Taylor, R.B., Solomon, S., Christian, H.A., Forbes, D.L., 1998. Potential impacts of global sea level rise on Canadian coast. The Canadian Geographer/Le Géographe canadien 42 (4), 365–379.
Shennan, I., 1986. Flandrian sea-level changes in the Fenland. II: tendencies of sea-level movement, altitudinal changes, and local and regional factors. J. Quat. Sci. 1 (2), 155–179.
Shennan, I., Horton, B., 2002. Holocene land-and sea-level changes in Great Britain. J. Quat. Sci. 17 (5-6), 511–526.
Shennan, I., Bradley, S., Milne, G., Brooks, A., Bassett, S., Hamilton, S., 2006. Relative sea-level changes, glacial isostatic modelling and ice-sheet reconstructions from the British Isles since the Last Glacial Maximum. J. Quat. Sci. 21 (6), 585–599.
Shennan, I., Lambeck, K., Horton, B., Innes, J., Lloyd, J., McArthur, J., Purcell, T., Rutherford, M., 2000. Late Devensian and Holocene records of relative sea- level changes in northwest Scotland and their implications for glacio-hydro- isostatic modelling. Quat. Sci. Rev. 19 (11), 1103–1135.
Shennan, I., Long, A.J., Horton, B.P., 2015. Handbook of Sea-level Research. John Wiley Sons.
Simon, K.M., James, T.S., Forbes, D.L., Telka, A.M., Dyke, A.S., Henton, J.A., 2014. A relative sea-level history for Arviat, Nunavut, and implications for Laurentide Ice-sheet thickness west of Hudson Bay. QR (Quat. Res.) (N. Y.) 82 (1), 185–197.
Simon, K.M., James, T.S., Henton, J.A., Dyke, A.S., 2016. A glacial isostatic adjustment model for the central and northern Laurentide Ice-sheet based on relative sea level and GPS measurements. Geophys. J. Int. 205 (3), 1618–1636.
Stea, R.R., Mott, R.J., 1989. Deglaciation environments and evidence for glaciers of younger Dryas age in Nova Scotia, Canada. Boreas 18 (2), 169–187.
Stokes, C.R., Clark, C.D., Storrar, R., 2009. Major changes in ice stream dynamics during deglaciation of the north-western margin of the Laurentide Ice-sheet. Quat. Sci. Rev. 28 (7), 721–738.
Stocchi, P., Spada, G., 2009. Influence of glacial isostatic adjustment upon current sea level variations in the Mediterranean. Tectonophysics 474 (1), 56–68.
Stopp, M.P., 1997. Long-term coastal occupancy between Cape Charles and trunmore bay, labrador. Arctic 119–137.
Stuiver, M., Polach, H.A., 1977. Discussion reporting of 14 C data. Radiocarbon 19 (3), 355–363.
Stuiver, M., Reimer, P.J., Reimer, R.W., 2017. CALIB 7.1 [WWW Program]. http://calib.org.
Svane, I., Ompi, M., 1993. Patch dynamics in beds of the blue mussel *Mytilus edulis* L.: effects of site, patch size, and position within a patch. Ophelia 37 (3), 187–202.
Tamura, T., 2012. Beach ridges and prograded beach deposits as palaeoenvironment records. Earth Sci. Rev. 114 (3), 279–297.
Tarasov, L., Peltier, W.R., 2004. A geophysically constrained large ensemble analysis of the deglacial history of the North American ice-sheet complex. Quat. Sci. Rev. 23 (3), 359–388.
Törnqvist, T.E., Rosenheim, B.E., Hu, P., Fernandez, A.B., 2015. Radiocarbon dating

and calibration. In: Shennan, I., Long, A.J., Horton, B.P. (Eds.), Handbook of Sea-level Research, pp. 349–360.
Törnqvist, T.E., Wallace, D.J., Storms, J.E., Wallinga, J., Van Dam, R.L., Blaauw, M., et al., 2008. Mississippi Delta subsidence primarily caused by compaction of Holocene strata. Nat. Geosci. 1 (3), 173–176.
Tucker, C., Leckie, D., McCann, S., 1982. Raised shoreline phenomena and postglacial emergence in south-central Newfoundland. Géogr. Phys. Quaternaire 36 (1–2), 165–174.
Ullman, D.J., Carlson, A.E., Hostetler, S.W., Clark, P.U., Cuzzone, J., Milne, G.A., et al., 2016. Final Laurentide ice-sheet deglaciation and Holocene climate-sea level change. Quat. Sci. Rev. 152, 49–59.
Vacchi, M., Marriner, N., Morhange, C., Spada, G., Fontana, A., Rovere, A., 2016. Multiproxy assessment of Holocene relative sea-level changes in the western Mediterranean: sea-level variability and improvements in the definition of the isostatic signal. Earth Sci. Rev. 155, 172–197.
Vacchi, M., Rovere, A., Chatzipetros, A., Zouros, N., Firpo, M., 2014. An updated database of Holocene relative sea level changes in NE Aegean Sea. Quat. Int. 328, 301–310.
van de Plassche, O., 1982. Sea-level Change and Water-level Movements in the Netherlands during the Holocene. Ph. D. dissertation. Vrije Universiteit, Amsterdam.
Vink, A., Steffen, H., Reinhardt, L., Kaufmann, G., 2007. Holocene relative sea-level change, isostatic subsidence and the radial viscosity structure of the mantle of northwest Europe (Belgium, The Netherlands, Germany, southern North Sea). Quat. Sci. Rev. 26 (25), 3249–3275.
Webb, D.J., 2014. On the tides and resonances of Hudson bay and Hudson strait. Ocean Sci. 10 (3), 411–426.
Whitehouse, P.L., Bentley, M.J., Le Brocq, A.M., 2012. A deglacial model for Antarctica: geological constraints and glaciological modelling as a basis for a new model of Antarctic glacial isostatic adjustment. Quat. Sci. Rev. 32, 1–24.
Woodroffe, S.A., Horton, B.P., 2005. Holocene sea-level changes in the Indo-Pacific. J. Asian Earth Sci. 25 (1), 29–43.
Wu, P., Peltier, W.R., 1982. Viscous gravitational relaxation. Geophys. J. Int. 70 (2), 435–485.
Wu, P., Peltier, W.R., 1984. Pleistocene deglaciation and the Earth's rotation: a new analysis. Geophys. J. Int. 76 (3), 753–791.
Zong, Y., 2004. Mid-holocene Sea-level highstand along the southeast coast of China. Quat. Int. 117 (1), 55–67.